Inorg. Chem. **2005**, *44*, 6591–6608

Organometallic Coordination Polymers Generated from Bent Bis(acetylenylphenyl)oxadiazole Ligands and Ag(I) Salts

Yu-Bin Dong,* Qiang Zhang, Le Wang, Jian-Ping Ma, Ru-Qi Huang, Da-Zhong Shen, and De-Zhan Chen

College of Chemistry, Chemical Engineering and Materials Science, and Shandong Key Lab of Chemical Functional Materials, Shandong Normal University, Jinan 250014, P. R. China

Received May 21, 2005

Two new bent oxadiazole bridging benzoacetylene ligands 2,5-bis(4-ethynylphenyl)-1,3,4-oxadiazole (**L9**) and 2,5-bis(3-ethynylphenyl)-1,3,4-oxadiazole (**L10**) were synthesized. The coordination chemistry of them with various inorganic Ag(I) salts has been investigated. Seven new coordination polymers were prepared by solution reactions and fully characterized by infrared spectroscopy, elemental analysis, and single-crystal X-ray diffraction. $[Ag_2(\mathbf{L9})](SO_3CF_3)_2$ (**1**) (triclinic, $P\bar{1}$; a =10.292(4), b = 10.794(4), c = 11.399(5) Å; α = 98.894(5), β = 102.360(6), γ = 90.319(5)°; Z = 2), $[Ag(\mathbf{L9})]SbF_6$ (**2**) (orthorhombic, *Cmca*; a = 19.059(9), b = 12.922(6), c = 15.609(7) Å; Z = 8), $[Ag(\mathbf{L9})]BF_4$ (**3**) (orthorhombic, *Cmca*; a = 19.128(3), b = 12.6042(18), c = 28.003(4) Å; Z = 16), $[Ag(\mathbf{L9})]ClO_4$ (**4**) (monoclinic, $P2_1/c$; a = 8.5153(16), b = 19.722(4), c = 10.320(2) Å; β = 105.307(3)°; Z = 4), $[Ag(\mathbf{L10})]SO_3CF_3$ (**5**) (triclinic, $P\bar{1}$; a = 9.0605(13), b = 10.4956(15), c = 10.8085(16) Å; α = 101.666(2), β = 109.269(2), γ = 100.944(2)°; Z = 2), $[Ag(\mathbf{L10})(H_2O)_{0.5}]BF_4 \cdot 0.5H_2O$ (**6**) (monoclinic, $C2/m$; a = 32.180(6), b = 17.027(3), c = 8.1453(15) Å; β = 102.541(3)°; Z = 8), and $\{[Ag_2(\mathbf{L10})_2(H_2O)](ClO_4)_2\} \cdot o$-xylene (**7**) (monoclinic, $P2_1/c$; a = 8.1460(10), b = 17.326(2), c = 30.345(4) Å; β = 97.71°; Z = 4) were obtained by the combination of **L9** and **L10** with various Ag(I) salts in a benzene/methylene chloride mixed solvent system. In addition, the luminescent and electrical conductive properties of these new compounds were investigated.

Introduction

The use of soluble inorganic transition metal salts or unsaturated transition metal coordination complexes in combination with organic bidentate or multidentate ligands as precursors to organic−inorganic coordination polymers or supramolecular complexes is a rapidly growing area of interest.[1] These materials not only exhibit encouraging potential applications[2,3] but also generate new insights into structural diversity. In this context, metal−heteroatoms (such as N atoms) and metal−carbon or metal−π interactions could be considered as the two most important interactions in the

* To whom correspondence should be addressed. E-mail: yubindong@sdnu.edu.cn.

(1) (a) Zaworotko, M. J.; Moulton, B. *Chem. Rev.* **2001**, *101*, 2619. (b) Eddaoudi, M.; Moler, D. B.; Li, H.; Chen, B.; Reineke, T. M.; Keeffe, M. O.; Yaghi, O. M. *Acc. Chem. Res.* **2001**, *34*, 319. (c) Constable, E. C. *Prog. Inorg. Chem.* **1994**, *42*, 67. (d) Dunbar, K. R.; Heintz, K. R. *Prog. Inorg. Chem.* **1996**, 283. (e) Whiteford, J. A.; Rachlin, E. M.; Stang, P. J. *Angew. Chem., Int. Ed. Engl.* **1996**, *35*, 2524. (f) Hagrman, P. J.; Hagrman, D.; Zubieta, J. *Angew. Chem., Int. Ed.* **1999**, *38*, 2639. (g) Blake, A. J.; Champness, N. R.; Hubberstey, P.; Li, W.-S.; Withersby, M. A.; Schröder, M. *Coord. Chem. Rev.* **1999**, *183* 117. (h) Batten, S.; Robson, R. *Angew. Chem., Int. Ed.* **1998**, *37*, 1460. (i) Barnett, S. A.; Champness, N. R. *Coord. Chem. Rev.* **2003**, *246*, 145.

(2) (a) Gardner, G. B.; Venkataraman, D.; Moore, J. S.; Lee, S. *Nature* **1995**, *374*, 792. (b) Kobel, W.; Hanack, M. *Inorg. Chem.* **1986**, *25*, 103. (c) Kato, R.; Kobayashi, H.; Kobayashi, A. *J. Am. Chem. Soc.* **1989**, *111*, 5224. (d) Sinzger, K.; Hünig, S.; Jopp, M.; Bauer, D.; Bietsch, W.; von Schütz, J. U.; Wolf, H. C.; Kremer, R. K.; Metzenthin, T.; Bau, R.; Khan, S. I.; Lindaum, A.; Lengauer, C. L.; Tillmanns, E. *J. Am. Chem. Soc.* **1993**, *115*, 7696. (e) Erk, P.; Gross, H.-J.; Hünig, U. L.; Meixner, H.; Werner, H.-P.; von Schütz, J. U.; Wolf, H. C. *Angew. Chem., Int. Ed. Engl.* **1989**, *28*, 1245. (f) Jung, O.; Pierpont, C. G. *J.* Am. Chem. Soc. **1994**, *116*, 2229. (g) Patoux, C.; Loudret, C.; Launay, L. P.; Joachim, C.; Gourdon, A. *Inorg. Chem.* **1997**, *36*, 5037. (e) Dybtsev, D. N.; Chun, H.; Yoon, S. H.; Kim, D.; Kim, K. *J. Am. Chem. Soc.* **2004**, *126*, 32. (h) Maji, T. K.; Uemura, K.; Chang, H.-C.; Matsuda, R.; Kitagawa, S. *J. Am. Chem. Soc.* **2004**, *126*, 3269.

(3) (a) Miyasaka, H.; Matsumoto, N.; Okawa, H.; Re, N.; Gallo, E.; Floriani, C. *J. Am. Chem. Soc.* **1996**, *118*, 981. (b) Kobayashi, H.; Tomita, H.; Naito, T.; Kobayashi, A.; Sakai, F.; Watanabe, T.; Cassoux, P. *J. Am. Chem. Soc.* **1996**, *118*, 368. (c) Sato, O.; Iyoda, T.; Fujishima, A.; Hashimoto, K. *Science* **1996**, *271*, 49. (d) Day, P. *Science* **1993**, *261*, 431. (c) Whiteside, G. M.; Mathias, J. P.; Seto, C. T. *Science* **1991**, *254*, 1312. (e) Bruce, D. W. *J. Chem. Soc., Dalton Trans.* **1993**, 2983. (f) Simon, J.; Engel, M. K.; Soulie, C. *New J. Chem.* **1992**, *16*, 287. (g) Dagani, R. *Chem. Eng. News* **1991**, *69* (May 27), 24.

10.1021/ic0508223 CCC: $30.25
Published on Web 08/20/2005

Chart 1. New and Known Five-Membered Heterocyclic Bridged Ligands Used by Us in Construction of Coordination Polymers

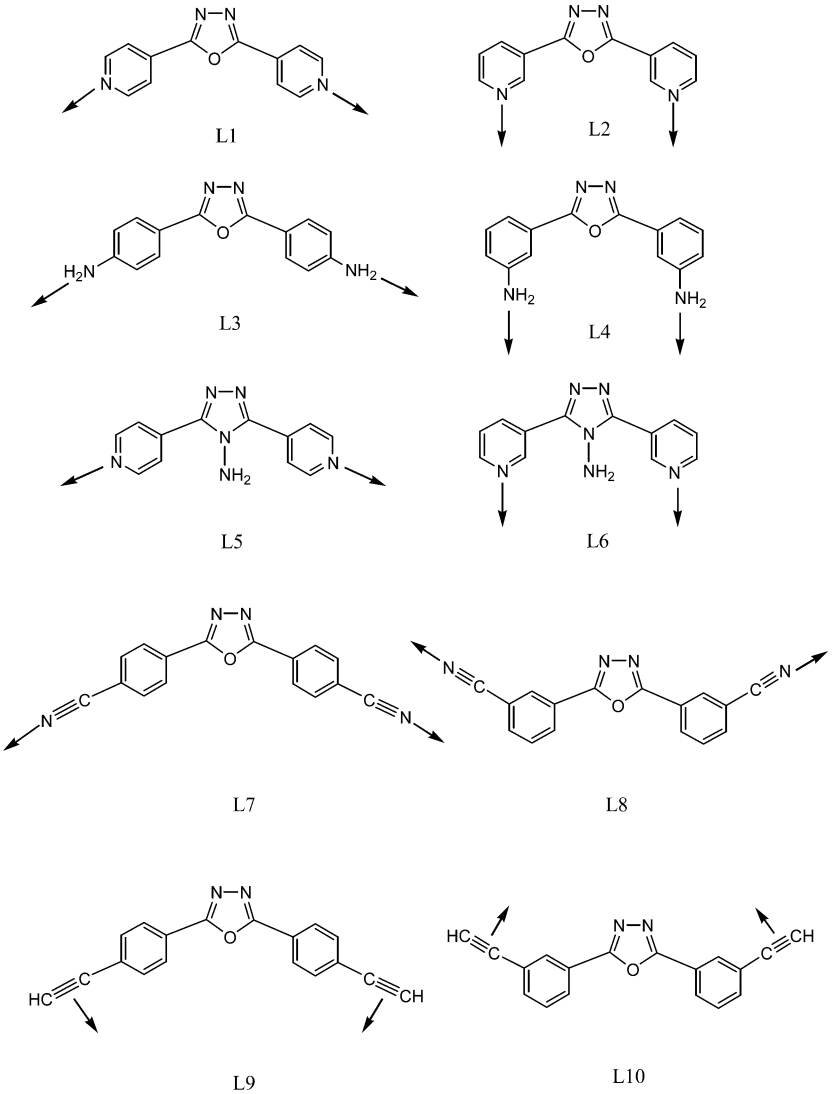

construction of polymeric architectures. Rigid and flexible organic bidentate and multidentate ligands with terminal N-donors as coordination sites separated by various spacers have been used in recent years and have resulted in a number of inorganic coordination polymers exhibiting a rich variety of structural motifs.[1] At the same time, smaller aromatic and polycyclic aromatic hydrocarbons (PAHs), acting as electron-donor species, were shown to be capable of incorporating metal ions into organometallic polymeric systems through cation$-\pi$ interactions, as was previously demonstrated well by many previous studies.[4] In contrast, the chemistry of polymeric compounds generated from multidenate organic ligands that can afford both heteroatoms and carbon atoms as coordination sites has received considerably less attention.[5,6]

Recently, we have design and synthesized a series of five-membered oxadiazole and triazole heteroatom cyclic rings bridging bent organic ligands with pyridyl-, cyano-, and aminophenyl groups as the terminal coordination sites (Chart 1). As a result of the specific geometry of these five-membered heterocyclic bridging ligands and of the coordination preferences of transition metals, various new coordination polymers have been obtained, some with open channels and interesting luminescent properties.[7] As we know, bent rigid ligands do not propagate the metal coordination code legibly into metal$-$organic architectures, which will make it somewhat more difficult to forecast the coordination network topologies.

(4) Munakata, M.; Wu, L. P.; Ning, G. L. *Coord. Chem. Rev*. **2000**, *198*, 171 and references therein.

(5) (a) Mayr, A.; Guo, J. *Inorg. Chem*. **1999**, *38*, 921. (b) Mayr, A.; Mao, Li. F. *Inorg. Chem.* **1998**, *37*, 5776. (c) Mao, L. F.; Mayr, A. *Inorg. Chem*. **1996**, *35*, 3183. (c) Reger, D. L.; Semeniuc, R. F.; Smith, M. D. *Inorg. Chem. Commun.* **2002**, *5*, 278.

(6) Recently we designed and synthesized a series of symmetric and unsymmetric fulvene ligands which can coordinate metal ions with both heteroatoms and π-donors as coordination sites; see the following: (a) Dong, Y.-B.; Jin, G.-X.; Smith, M. D.; Huang, R.-Q.; Tong, B.; zur Loye, H.-C. *Inorg. Chem.* **2002**, *41*, 4909. (b) Dong, Y.-B.; Ma, J.-P.; Jin, G.-X.; Huang, R.-Q.; Smith, M. D. *Dalton Trans*. **2003**, *22*, 4324. (c) Dong, Y.-B.; Zhao, X.; Jin, G.-X.; Huang, R.-Q.; Smith, M. D. *Eur. J. Inorg. Chem.* **2003**, *22*, 4017. (d) Dong, Y.-B.; Jin, G.-X.; Zhao, X.; Huang, R.-Q.; Smith, M. D.; Stitzer, K. E.; zur Loye, H.-C. *Organometallics* **2004**, *23*, 1604. (e) Dong, Y.-B.; Wang, P.; Huang, R.-Q.; Smith, M. D. *Inorg. Chem.* **2004**, *43*, 4727. (f) Wang, P.; Dong, Y.-B.; Huang, R.-Q.; Smith, M. D. *Cryst. Growth Des*. **2005**, *5*, 701. (g) Dong, Y.-B.; Geng, Y.; Ma, J.-P.; Huang, R.-Q. *Inorg. Chem*. **2005**, *44*, 1693.

The carbon−carbon triple bond is classical organometallic coordinating group with a rich diversity of modes of metal−carbon bonding.[8] So far, a number of novel binuclear, multinuclear, polymeric, and catenane-like Au(I) and Cu(I) complexes based on substituted ethynyl anion ligands have been reported.[9] In contrast, silver(I) acetylide compounds based on silver−ethynyl (HC≡C$^-$) and silver−ethynediyl ($^-$C≡C$^-$) binding are less studied.[9a,b] This is probably due to their instabilities with regard to light-induced decomposition reactions. To our knowledge, the coordination chemistry based on bridged organic ligands with a neutral π-ethynyl terminal group is still an undeveloped field. The idea herein is to combine a five-membered oxadiazole ring with substituted −C≡CH as a terminal coordination moiety to generate new types of bent ligands by a Pd-catalyzed coupling reaction (Scheme 1).[10] It is expected that the polymeric complexes based on such kinds of ligands could be driven by both metal−heteroatom and metal−carbon or metal−π coordination interactions. On the other hand, the coordination orientation of π-donors on this type of ligands is distinctly different from the known five-membered bridged organic spacers (Chart 1), which would bring on the coordination polymeric complexes with new patterns.

In this paper we wish to report on the synthesis of new ligands **L9** and **L10** and a series of new Ag(I)-containing organometallic polymeric complexes $[Ag_2(\mathbf{L9})](SO_3CF_3)_2$ (**1**), $[Ag(\mathbf{L9})]ClO_4$ (**2**), $[Ag(\mathbf{L9})]SbF_6$ (**3**), $[Ag(\mathbf{L9})]BF_4$ (**4**), $[Ag(\mathbf{L10})]SO_3CF_3$ (**5**), $[Ag(\mathbf{L10})(H_2O)_{0.5}]BF_4\cdot 0.5H_2O$ (**6**), and $\{[Ag_2(\mathbf{L10})_2(H_2O)](ClO_4)_2\}\cdot o$-xylene (**7**) based on both metal−π and metal−nitrogen coordination interactions.

Experimental Section

Materials and Methods. $AgSO_3CF_3$, $AgClO_4$, $AgBF_4$, and $AgSbF_6$ (Acros) were used as obtained without further purification. Infrared (IR) samples were prepared as KBr pellets, and spectra were obtained in the 400−4000 cm^{-1} range using a Perkin-Elmer 1600 FTIR spectrometer. Elemental analyses were performed on a Perkin-Elmer model 2400 analyzer. ^{1}H NMR data were collected using an AM-300 spectrometer. Chemical shifts are reported in δ relative to TMS. All fluorescence measurements were carried out on a Cary Eclipse spectrofluorometer (Varian, Australia) equipped with a xenon lamp and quartz carrier at room temperature. Thermogravimetric analyses were carried out using a TA Instrument SDT 2960 simultaneous DTA-TGA under flowing nitrogen at a heating rate of 10 °C/min. Electrical conductivity was performed on Agilent Technologies (4294A-ATO-20150). XRD pattern were obtained on a D8 ADVANCE X-ray powder diffraction (XRD) with Cu Kα radiation (λ = 1.5405 Å).

Caution! Two of the crystallization procedures involve $AgClO_4$, which is a strong oxidizer.

Preparation of L9. To a solution of **S1** (2.50 g, 5.27 mmol) and HC≡CSiMe$_3$ (1.65 mL, 12 mmol) in triethylamine (100 mL) were added $Pd(PPh_3)Cl_2$ (89.5 mg, 0.58 mmol) and CuI (72.7 mg, 0.26 mmol). The mixture was stirred overnight at room temperature. After removal the solvent under vacuum, the residue was purified on silica gel by column using CH_2Cl_2 as the eluent to give 2,5-bis(4-((trimethylsilyl)ethynyl)phenyl)-1,3,4-oxadiazole as a white solid (yield 97%). The white solid obtained was added to a methanol solution of potassium hydroxide. The mixture was stirred for 24 h at room temperature. After the hydrolysis was complete (monitored by TLC), the solvent was removed under vacuum and the residue was purified by chromatograpy on silica gel using methylene chloride as the eluent to afford a light yellow solid. Yield: 1.29 g, 90%. Mp: 210−211 °C. ^{1}H NMR (300 MHz, DMSO-d_6, 25 °C, TMS, ppm): 8.10 (d, 4H, −C$_6$H$_4$), 7.68 (d, 4H, −C$_6$H$_4$), 4.46 (s, 2H, −C≡CH). IR (KBr, cm^{-1}): 3286 (s), 2170 (w), 1933 (s), 1609 (w), 1572 (m), 1483 (s), 1263 (m), 1099 (s), 1076 (m), 848 (s), 747 (s), 708 (s), 679 (s), 620 (s), 537 (m). Anal. Calcd for $C_{18}H_{10}N_2O$ (**L9**): C, 80.00; H, 3.70; N, 10.37. Found: C, 79.79; H, 3.80; N, 10.34. UV−vis spectrum (in CH_3CN at room temperature): λ_{max} = 308 nm.

Preparation of L10. To a solution of **S2** (1.42 g, 3.0 mmol) and HC≡CC(Me)$_2$OH (0.64 mL, 6.6 mmol) in triethylamine (30 mL) were added THF (8 mL), $Pd(PPh_3)Cl_2$ (46.0 mg, 0.066 mmol), and CuI (38.0 mg, 0.20 mmol). The mixture was stirred overnight at room temperature. After removal of the solvent under vacuum, the residue was purified on silica gel by column using CH_2Cl_2/CH_3CO_2Et (2:1, v/v) as the eluent to give 2,5-bis[4-(2′-methyl-3′-butyn-2′-olphenyl)]-1,3,4-oxadiazole as a white solid (yield 95%). The white solid obtained was added to a benzene solution of sodium hydroxide. The mixture was refluxed for 2 h. After the hydrolysis was complete (monitored by TLC), the solvent was removed under vacuum and the residue was purified by chromatograpy on silica

(7) (a) Dong, Y.-B.; Ma, J.-P.; Smith, M. D.; Huang, R.-Q.; Tang, B.; Chen, D.; zur Loye, H.-C. *Solid State Sci.* **2002**, *4*, 1313. (b) Dong, Y.-B.; Ma, J.-P.; Huang, R.-Q.; Smith, M. D.; zur Loye, H.-C. *Inorg. Chem.* **2003**, *42*, 294. (c) Dong, Y.-B.; Ma, J.-P.; Smith, M. D.; Huang, R.-Q.; Tang, B.; Guo, D.-S.; Wang, J.-S.; zur Loye, H.-C. *Solid State Sci.* **2003**, *5*, 601. (d) Dong, Y.-B.; Ma, J.-P.; Smith, M. D.; Huang, R.-Q.; Wang, J.-S.; zur Loye, H.-C. *Solid State Sci.* **2003**, *5*, 1177. (e) Dong, Y.-B.; Cheng, J.-Y.; Wang, H.-Y.; Huang, R.-Q.; Tang, B.; Smith, M. D.; zur Loye, H.-C. *Chem. Mater.* **2003**, *15*, 2593. (f) Dong, Y.-B.; Ma, J.-P.; Huang, R.-Q.; Liang, F.-Z.; Smith, M. D. *Dalton Trans.* **2003**, *9*, 1472. (g) Dong, Y.-B.; Cheng, J.-Y.; Huang, R.-Q.; Tang, B.; Smith, M. D.; zur Loye, H.-C. *Inorg. Chem.* **2003**, *42*, 5699. (h) Cheng, J.-Y.; Dong, Y.-B.; Ma, J.-P.; Huang, R.-Q.; Smith, M. D. *Inorg. Chem. Commun.* **2005**, *8*, 6. (i) Dong, Y.-B.; Cheng, J.-Y.; Huang, R.-Q.; Smith, M. D. *Inorg. Chim. Acta* **2005**, *358*, 891. (j) Dong, Y.-B.; Cheng, J.-Y.; Ma, J.-P.; Huang R.-Q.; Smith, M. D. *Cryst. Growth Des.* **2005**, *5*, 585. (k) Dong, Y.-B.; Wang, H.-Y.; Ma, J.-P.; Huang, R.-Q.; Smith, M. D. *Cryst. Growth Des.* **2005**, 5, 789. (l) Wang, P.; Dong, Y.-B.; Ma, J.-P.; Huang, R.-Q.; Smith, M. D. *Inorg. Chem. Commun.* **2005**, *8*, 596. (m) Dong, Y.-B.; Wang, H.-Y.; Ma, J.-P.; Shen, D.-Z.; Huang, R.-Q. *Inorg. Chem.* **2005**, *44*, 4679. (n) Ma, J. P.; Dong, Y.-B.; Huang, R.-Q.; Smith, M. D.; Cheng, Y. S. *Inorg Chem.* **2005**, *44*, 6143.

(8) (a) Green, M. L. H. *Organometallic Compounds*, 3rd ed.; Chapman and Hall Ltd.: London, 1968; Vol. 2, The Transition Elements. (b) Pearson, A. J. *Metallo-organic Chemistry*; Wiley: New York, 1985. (c) Crabtree, R. H. *The Organometallic Chemistry of the Transition Metals*, 2nd ed.; Wiley: New York, 1994. (d) Collman, J. P.; Hegedus, L.; Norton, J. R.; Finke, R. G. *Principles and Applications of Organotransition Metal Chemistry*; University Science: Mill Valley, CA, 1987. (e) Spessard, G. O.; Miessler, G. L. *Organometallic Chemistry*; Prentice Hall: Upper Saddle River, NJ, 1997. (f) Cotton, F. A.; Wilkinson, G. *Advanced Inorganic Chemistry*, 5th ed.; Interscience Publishers: New York, 1988.

(9) (a) Wang, Q.-M.; Mak, T. C. W. *J. Am. Chem. Soc.* **2001**, *123*, 7594. (b) Zhao, L.; Mak, T. C. W. *J. Am. Chem. Soc.* **2004**, *126*, 6852. (c) Jia, G.; Puddephatt, R. J.; Scott, J. D.; Vittal, J. J. *Organometallics* **1993**, *12*, 3565. (d) Irwin, M. J.; Jia, G.; Payne, N. C.; Puddephatt, R. J. *Organometallics* **1996**, *15*, 51. (e) McArdle, C. P.; Irwin, M. J.; Jennings, M. C.; Puddephatt, R. J. *Angew. Chem., Int. Ed.* **1999**, *38*, 3376. (f) McArdle, C. P.; Vittal, J. J.; Puddephatt, R. J. *Angew. Chem., Int. Ed.* **2000**, *39*, 3819. (g) Yam, V. W. W.; Choi, S. W. K.; Cheung, K. K. *Organometallics* **1996**, *15*, 1734. (h) Lin, Y.-Y.; Lai, S.-W.; Che, C.-M.; Cheung, K.-K.; Zhou, Z.-Y. *Organometallics* **2002**, *21*, 2275. (i) Reger, D. L.; Huff, M. F. *Organometallics* **1992**, *11*, 69. (j) Knotter, D. M.; Spek, A. L.; Grove, D. M.; van Koten, G. *Organometallics* **1992**, *11*, 4083.

(10) Bunz, U. H. F. *Chem. Rev.* **2000**, *100*, 1605.

Scheme 1. Synthesis of New Ligands **L9** and **L10** and Compounds **1**−**7**

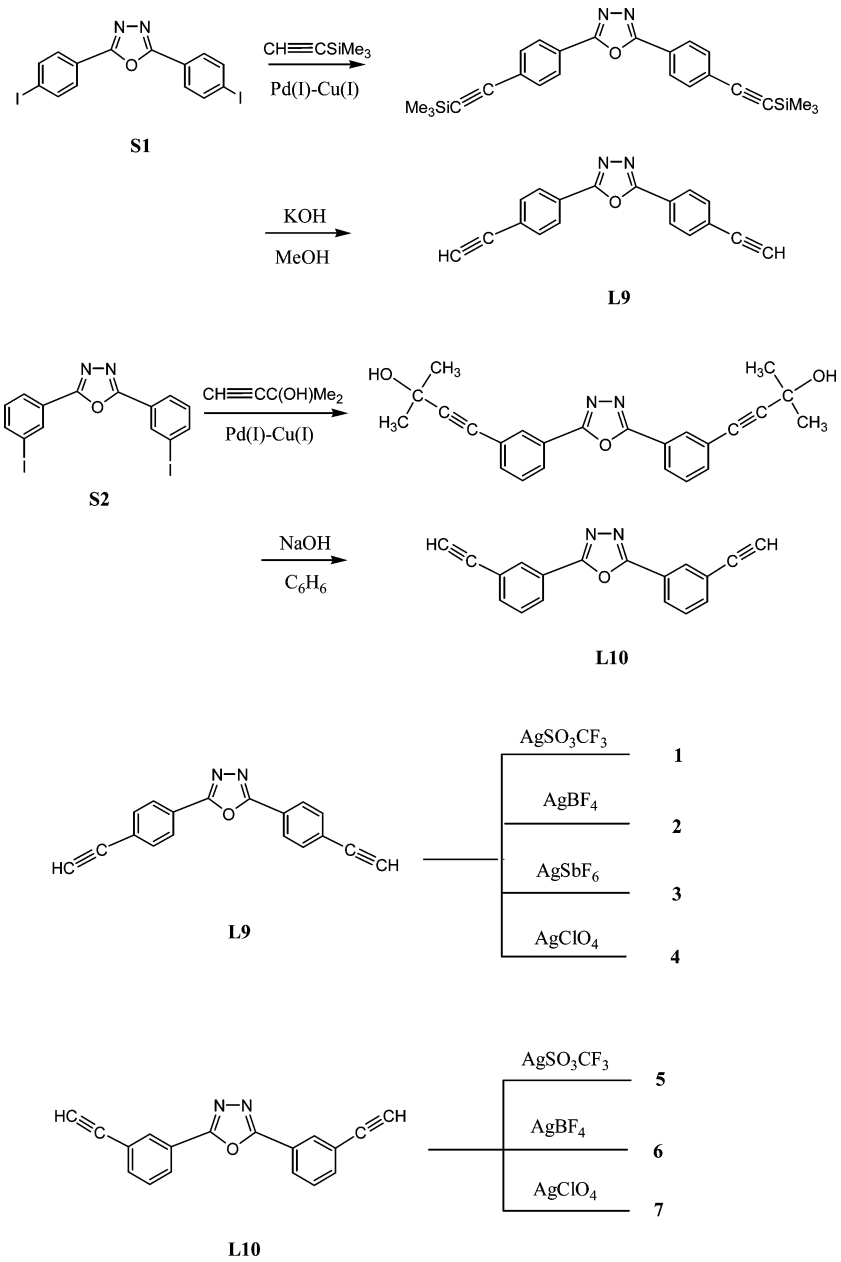

gel using methylene chloride as the eluent to afford a light yellow solid. Yield: 0.66 g, 85%. Mp: 180−182 °C. ^{1}H NMR (300 MHz, DMSO-d_6, 25 °C, TMS, ppm): 8.25 (s, 2H, −C_6H_4), 8.20 (d, 2H, −C_6H_4), 7.75 (d, 2H, −C_6H_4), 7.65 (t, 2H, −C_6H_4), 4.41 (s, 2H, −C≡CH). IR (KBr, cm^{-1}): 3277 (s), 2169 (w), 1638 (s), 1618 (s), 1541 (m), 1401 (s), 902 (w), 840 (w), 807 (w), 734 (w), 670 (w), 620 (m), 478 (m). Anal. Calcd for $C_{18}H_{10}N_2O$ (**L10**): C, 80.00; H, 3.70; N, 10.37. Found: C, 79.87; H, 3.39; N, 10.16. UV−vis spectrum (in CH_3CN at room temperature): λ_{max} = 278 nm.

Preparation of [Ag$_2$(L9)](SO$_3$CF$_3$)$_2$ (1). A solution of $AgSO_3CF_3$ (25.6 mg, 0.10 mmol) in benzene (8 mL) was layered onto a solution of **L9** (27.0 mg, 0.10 mmol) in CH_2Cl_2 (8 mL). The sloutions were left for about 2 days at room temperature, and colorless crystals were obtained. Yield: 87%. IR (KBr, cm^{-1}): 3288 (s), 2170 (w), 2111 (w), 1608 (s), 1574 (s), 1548 (s), 1490 (s), 1403 (s), 1281 (vs), 1244 (s), 1179 (s), 1022 (s), 846 (s), 746 (s), 706 (m), 628 (s), 536 (m), 515 (m). ^{1}HNMR (300 MHz, DMSO-d_6, 25 °C, TMS, ppm): 8.13 (d, 4H, −C_6H_4), 7.70 (d, 4H, −C_6H_4), 4.47 (s, 2H, −C≡CH). Anal. Calcd for $C_{24}H_{10}Ag_2F_6N_2O_7S_2$: C, 30.61; H, 1.28; N, 3.57. Found: C, 30.52; H, 1.21; N, 3.23. UV−vis spectrum (in CH_3CN at room temperature): λ_{max} = 308 nm.

Preparation of [Ag(L9)]ClO$_4$ (2). A solution of $AgClO_4$ (20.7 mg, 0.10 mmol) in benzene (8 mL) was layered onto a solution of **L9** (27.0 mg, 0.10 mmol) in CH_2Cl_2 (8 mL). The sloutions were left for about 2 days at room temperature, and colorless crystals were obtained. Yield: 86%. IR (KBr, cm^{-1}): 3287 (s), 2170 (w), 2105(w), 1608 (s), 1546 (s), 1488 (s), 1404 (s), 1264 (vs), 1022 (s), 846 (s), 746 (s), 625 (s), 577 (m), 517 (s). ^{1}H NMR (300 MHz, DMSO-d_6, 25 °C, TMS, ppm): 8.13 (d, 4H, −C_6H_4), 7.72 (d, 4H, −C_6H_4), 4.48 (s, 2H, −C≡CH). Anal. Calcd for $C_{18}H_{10}AgClN_2O_5$: C, 45.28; H, 2.10; N, 5.87. Found: C, 45.22; H, 2.00; N, 5.61. UV−vis spectrum (in CH_3CN at room temperature): λ_{max} = 302 nm.

Preparation of [Ag(L9)]SbF$_6$ (3). A solution of $AgSbF_6$ (34.4 mg, 0.10 mmol) in benzene (8 mL) was layered onto a solution of **L9** (27.0 mg, 0.10 mmol) in CH_2Cl_2 (8 mL). The sloutions were left for about 2 days at room temperature, and colorless crystals were obtained. Yield: 86%. IR (KBr, cm^{-1}): 3286 (m), 2078 (w),

Table 1. Crystallographic Data for **L10** and **1**−**3**[a]

param	**L10**	**1**	**2**	**3**
empirical formula	$C_{18}H_{10}N_2O$	$C_{20}H_{10}Ag_2F_6N_2O_7S_2$	$C_{18}H_{10}AgF_6N_2OSb$	$C_{18}H_{10}AgBF_4N_2O$
fw	270.28	784.16	613.90	464.96
cryst syst	monoclinic	triclinic	orthorhombic	orthorhombic
a (Å)	31.405(7)	10.292(4)	19.059(9)	19.128(3)
b (Å)	6.2903(14)	10.794(4)	12.922(6)	12.6042(18)
c (Å)	15.406(3)	11.399(5)	15.609(7)	28.003(4)
a (deg)	90	98.894(5)	90	90
b (deg)	118.656(3)	102.360(6)	90	90
g (deg)	90	90.319(5)	90	90
V (Å^3)	2670.6(10)	1221.2(8)	3844(3)	6751.5(16)
space group	*C*2/*c*	$P\bar{1}$	*Cmca*	*Cmca*
Z value	8	2	8	16
ρ_{calcd} (g/cm^3)	1.344	2.133	2.121	1.830
μ(Mo Kα) (mm^{-1})	0.085	1.866	2.492	1.246
temp (K)	293(2)	293(2)	293(2)	293(2)
no. of observns ($I > 3\sigma(I)$)	2482	4424	1847	3238
final R indices [$I > 2\sigma(I)$]: R; R_w	0.0457; 0.1133	0.0559; 0.1513	0.0738; 0.1736	0.0683; 0.1764

[a] $R1 = \Sigma||F_o| - |F_c||/\Sigma|F_o|$. $wR2 = \{\Sigma[w(F_o^2 - F_c^2)^2]/\Sigma[w(F_o^2)^2]\}^{1/2}$.

1609 (m), 1545 (m), 1488 (s), 1402 (s), 1261 (vs), 1026 (s), 846 (s), 746 (s), 648 (s), 624 (s), 578 (w), 517 (m). ^{1}H NMR (300 MHz, DMSO-d_6, 25 °C, TMS, ppm): 8.12 (d, 4H, $-C_6H_4$), 7.69 (d, 4H, $-C_6H_4$), 4.47 (s, 2H, $-C\equiv CH$). Anal. Calcd for $C_{18}H_{10}AgF_6N_2OSb$: C, 35.20; H, 1.63; N, 4.56. Found: C, 35.52; H, 1.41; N, 4.43. UV−vis spectrum (in CH_3CN at room temperature): λ_{max} = 304 nm.

Preparation of [Ag(L9)]BF$_4$ (4). A solution of $AgBF_4$ (19.5 mg, 0.10 mmol) in benzene (8 mL) was layered onto a solution of **L9** (27.0 mg, 0.10 mmol) in CH_2Cl_2 (8 mL). The sloutions were left for about 2 days at room temperature, and colorless crystals were obtained. Yield: 87%. IR (KBr, cm^{-1}): 3288 (vs), 2072 (w), 1638 (w), 1619 (w), 1573 (w), 1545 (s), 1486(m), 1400 (s), 1265 (m), 1100 (s), 847(s), 747 (s), 707 (m), 677 (m), 654 (s), 621 (s), 536 (s). ^{1}H NMR (300 MHz, DMSO-d_6, 25 °C, TMS, ppm): 8.13 (d, 4H, $-C_6H_4$), 7.72 (d, 4H, $-C_6H_4$), 4.48 (s, 2H, $-C\equiv CH$). Anal. Calcd for $C_{18}H_{10}AgBF_4N_2O$: C, 46.45; H, 2.15; N, 6.02. Found: C, 46.75; H, 2.45; N, 6.33. UV−vis spectrum (in CH_3CN at room temperature): λ_{max} = 308 nm.

Preparation of [Ag(L10)]SO$_3$CF$_3$ (5). A solution of $AgSO_3CF_3$(25.6 mg, 0.10 mmol) in benzene (8 mL) was layered onto a solution of **L10** (27.0 mg, 0.10 mmol) in CH_2Cl_2 (8 mL). The sloutions were left for about 3 days at room temperature, and colorless crystals were obtained. Yield: 86%. IR (KBr, cm^{-1}): 3253 (s), 2170 (w), 2098 (w), 1638 (s), 1620 (s), 1542 (s), 1402 (s), 1264 (s), 1158 (s), 1086 (m), 1029 (s), 902 (m), 822 (m), 802 (m), 737 (m), 682 (m), 626 (s), 513 (m). ^{1}H NMR (300 MHz, DMSO-d_6, 25 °C, TMS, ppm): 8.24 (s, 2H, $-C_6H_4$), 8.18 (d, 2H, $-C_6H_4$), 7.74 (d, 2H, $-C_6H_4$), 7.64 (t, 2H, $-C_6H_4$), 4.40 (s, 2H, $-C\equiv CH$). Anal. Calcd for $C_{19}H_{10}Ag\ F_3N_2O_4S$: C, 40.99; H, 1.90; N, 5.31. Found: C, 41.34; H, 1.59; N, 5.12. UV−vis spectrum (in CH_3CN at room temperature): λ_{max} = 280 nm.

Preparation of [Ag(L10)(H$_2$O)$_{0.5}$]BF$_4$·0.5H$_2$O (6). A solution of $AgBF_4$ (19.5 mg, 0.10 mmol) in benzene (8 mL) was layered onto a solution of **L10** (27.0 mg, 0.10 mmol) in CH_2Cl_2 (8 mL). The sloutions were left for 1 day at room temperature, and colorless crystals were obtained. Yield: 85%. IR (KBr, cm^{-1}): 3276 (s), 2169 (w), 2107(w), 1638 (s), 1618 (s), 1544 (m), 1401 (s), 1084 (s), 913 (w), 842 (w), 805 (w), 737 (w), 682 (m), 624 (m), 478 (w). ^{1}H NMR (300 MHz, DMSO-d_6, 25 °C, TMS, ppm): 8.25 (s, 2H, $-C_6H_4$), 8.20 (d, 2H, $-C_6H_4$), 7.76 (d, 2H, $-C_6H_4$), 7.65 (t, 2H, $-C_6H_4$), 4.41 (s, 2H, $-C\equiv CH$). Anal. Calcd for $C_{18}H_{12}AgBF_4N_2O_2$: C, 44.72; H, 2.48; N, 5.80. Found: C, 44.24; H, 2.59; N, 5.55. UV−vis spectrum (in CH_3CN at room temperature): λ_{max} = 284 nm.

Preparation of {[Ag$_2$(L10)$_2$(H$_2$O)](ClO$_4$)$_2$}·*o*-xylene (7). A solution of $AgClO_4$ (20.7 mg, 0.10 mmol) in benzene (8 mL) was layered onto a solution of **L10** (27.0 mg, 0.10 mmol) in CH_2Cl_2 (8 mL). The sloutions were left for 3 days at room temperature, and colorless crystals were obtained. Yield: 85%. IR (KBr, cm^{-1}): 3257 (s), 2169 (w), 2109 (w), 1639 (s), 1617 (s), 1549 (m), 1401 (s), 1111 (s), 890 (w), 841(w), 806 (w), 738 (m), 679 (w), 620 (s), 473 (w). ^{1}H NMR (300 MHz, DMSO-d_6, 25 °C, TMS, ppm): 8.24 (s, 2H, $-C_6H_4$), 8.19 (d, 2H, $-C_6H_4$), 7.74 (d, 2H, $-C_6H_4$), 7.64 (t, 2H, $-C_6H_4$), 7.02−7.18 (m, 4H, $-C_6H_4$), 4.41 (s, 2H, $-C\equiv CH$), 2.19 (s, 6H, $-CH_3$). Anal. Calcd for $C_{26}H_{22}Ag_2Cl_2N_2O_{10}$: C, 26.70; H, 1.48; N, 3.46. Found: C, 27.15; H, 1.23; N, 3.26. UV−vis spectrum (in CH_3CN at room temperature): λ_{max} = 282 nm.

Single-Crystal Structure Determination. Suitable single crystals of **1**−**7** were selected and mounted in air onto thin glass fibers. X-ray intensity data were measured at 150 K on a Bruker SMART APEX CCD-based diffractometer (Mo Kα radiation, λ = 0.710 73 Å). The raw frame data for **1**−**7** were integrated into SHELX-format reflection files and corrected for Lorentz and polarization effects using SAINT.[11] Corrections for incident and diffracted beam absorption effects were applied using SADABS.[11] None of the crystals showed evidence of crystal decay during data collection. All structures were solved by a combination of direct methods and difference Fourier syntheses and refined against F^2 by the full-matrix least-squares technique. Crystal data, data collection parameters, and refinement statistics for **1**−**7** are listed in Tables 1 and 2. Relevant interatomic bond distances and bond angles for **1**−**7** are given in Tables 3−9.

Results and Discussion

Synthesis and Structural Analysis of Ligands L9 and L10. L9 and **L10** were synthesized by a Pd-catalyzed reaction. They can be considered as new members of the bent five-membered heterocyclic ring-bridging organic ligands. Their structures have been fully characterized by infrared spectroscopy, elemental analysis, and ^{1}H NMR. To further confirm the structure of the new ligands, the solid molecular

(11) Bruker Analytical X-ray Systems, Inc., Madison, WI, 1998.

Table 2. Crystallographic Data for **4**−**7**[a]

param	**4**	**5**	**6**	**7**
empirical formula	$C_{18}H_{10}AgClN_2O_5$	$C_{19}H_{10}AgF_3N_2O_4S$	$C_{18}H_{12}AgBF_4N_2O_2$	$C_{44}H_{32}Ag_2Cl_2N_4O_{11}$
fw	477.60	527.22	482.98	1079.38
cryst syst	monoclinic	triclinic	monoclinic	monoclinic
a (Å)	8.5153(16)	9.0605(13)	32.180(6)	8.1460(10)
b (Å)	19.722(4)	10.4956(15)	17.027(3)	17.326(2)
c (Å)	10.320(2)	10.8085(16)	8.1453(15)	30.345(4)
a (deg)	90	101.666(2)	90	90
b (deg)	105.307(3)	109.269(2)	102.541(3)	97.71
g (deg)	90	100.944(2)	90	90
V (Å^3)	999.97(19)	912.9(2)	4356.7(14)	4244.0(9)
space group	$P\bar{1}$	$P\bar{1}$	*C*2/*m*	$P2_1$/c
Z value	4	2	4	2
ρ_{calcd} (g/cm^3)	1.898	1.918	1.473	1.689
μ(Mo Kα) (mm^{-1})	1.401	1.280	0.972	1.116
temp (K)	293(2)	293(2)	293(2)	293(2)
no. of observns ($I > 3\sigma(I)$)	2939	3221	4141	8288
final R indices [$I > 2\sigma(I)$]: R; R_w	0.0728; 0.1458	0.0284; 0.0755	0.0720; 0.1718	0.0393; 0.1078

[a] $R1 = \sum||F_o| - |F_c||/\sum|F_o|$. $wR2 = \{\sum[w(F_o^2 - F_c^2)^2]/\sum[w(F_o^2)^2]\}^{1/2}$.

Table 3. Interatomic Distances (Å) and Bond Angles (deg) with Esd's in Parentheses for **1**[a]

Ag(1)−N(2)	2.369(5)	Ag(1)−O(6)#1	2.375(6)
Ag(1)−O(2)	2.464(6)	Ag(1)−O(7)	2.525(5)
Ag(1)−C(5)#2	2.532(8)	Ag(2)−N(1)	2.200(5)
Ag(2)−O(4)#3	2.303(6)	Ag(2)−O(4)	2.509(6)
Ag(2)−O(7)	2.640(5)		
N(2)−Ag(1)−O(6)#1	127.5(2)	N(2)−Ag(1)−O(2)	96.5(2)
O(6)#1−Ag(1) −O(2)	86.9(2)	N(2)−Ag(1)−O(7)	105.32(18)
O(6)#1−Ag(1)−O(7)	126.6(2)	O(2)−Ag(1)−O(7)	79.3(2)
N(2)−Ag(1)−C(5)#2	104.9(2)	O(6)#1−Ag(1)−C(5)#2	85.4(3)
O(2)−Ag(1)−C(5)#2	157.6(3)	O(7)−Ag(1)−C(5)#2	88.5(2)
N(1)−Ag(2)−O(4)#3	157.8(2)	N(1)−Ag(2)−O(4)	112.68(19)
O(4)#3−Ag(2)−O(4)	89.37(18)	N(1)−Ag(2)−O(7)	104.00(18)
O(4)#3−Ag(2)−O(7)	81.46(19)	O(4)−Ag(2)−O(7)	80.69(18)

[a] Symmetry transformations used to generate equivalent atoms: (#1) $-x + 1, -y + 1, -z$; (#2) $-x, -y + 2, -z$; (#3) $-x, -y + 1, -z$.

Table 4. Interatomic Distances (Å) and Bond Angles (deg) with Esd's in Parentheses for **2**[a]

Ag(1)−N(1)	2.281(7)	Ag(1)−C(7)#2	2.555(14)
N(1)−Ag(1)−N(1)#1	120.6(3)	N(1)−Ag(1)−C(7)#2	101.6(3)
N(1)#1−Ag(1)−C(7)#2	89.5(3)	N(1)−Ag(1)−C(7)#3	89.5(3)
N(1)#1−Ag(1)−C(7)#3	101.6(3)	C(7)#2−Ag(1)−C(7)#3	157.6(5)
C(1)−N(1)−N(1)#4	106.3(5)	C(1)−N(1)−Ag(1)	132.8(6)

[a] Symmetry transformations used to generate equivalent atoms: (#1) $x, -y, -z$; (#2) $-x + 3/2, -y + 1/2, -z$; (#3) $-x + 3/2, y - 1/2, z$; (#4) $-x + 2, y, z$; (#5) $-x, y, z$.

Table 5. Interatomic Distances (Å) and Bond Angles (deg) with Esd's in Parentheses for **3**[a]

Ag(1)−N(1)	2.316(5)	Ag(1)−N(2)	2.329(5)
Ag(1)−C(7)#1	2.434(8)	Ag(1)−C(16)#2	2.442(7)
Ag(1)−C(6)#1	2.671(6)		
N(1)−Ag(1)−N(2)	121.69(17)	N(1)−Ag(1)−C(7)$^{\#1}$	91.9(2)
N(2)−Ag(1)−C(7)#1	101.0(3)	N(1)−Ag(1)−C(16)#2	100.3(2)
N(2)−Ag(1)−C(16)#2	88.9(2)	C(7)#1−Ag(1)−C(16)#2	157.2(3)
N(1)−Ag(1)−C(6)#1	112.6(2)	N(2)−Ag(1)−C(6)#1	101.4(2)
C(7)#1−Ag(1)−C(6)#1	26.0(2)	C(16)#2−Ag(1)−C(6)#1	132.1(2)

[a] Symmetry transformations used to generate equivalent atoms: (#1) $-x + 1/2, y + 1/2, z$; (#2) $-x + 1/2, y - 1/2, z$. #3 $-x+1,y,z$ #4 $-x+2,y,z$

structure of **L10** was determined using single-crystal X-ray diffraction. As shown in Figure 1, the shape of the ligand is bent, which is similar to the known organic ligands of **L1**−**L8**. Two terminal benzoacetylene groups and a bridging

Table 6. Interatomic Distances (Å) and Bond Angles (deg) with Esd's in Parentheses for **4**[a]

Ag(1)−N(1)#1	2.257(5)	Ag(1)−N(2)	2.295(5)
Ag(1)−C(5)#2	2.473(8)	Ag(1)−O(2)	2.597(6)
N(1)#1−Ag(1) −N(2)	125.54(18)	N(1)#1−Ag(1)−C(5)#2	123.5(3)
N(2)−Ag(1)−C(5)#2	89.4(3)	N(1)#1−Ag(1)−O(2)	108.4(2)
N(2)−Ag(1)−O(2)	104.9(2)	C(5)#2−Ag(1)−O(2)	101.3(3)

[a] Symmetry transformations used to generate equivalent atoms: (#1) $-x + 1, -y + 1, -z + 1$; (#2) $x - 1, y, z - 1$; (#3) $x + 1, y, z + 1$.

Table 7. Interatomic Distances (Å) and Bond Angles (deg) with Esd's in Parentheses for **5**[a]

Ag(1)−N(1)#1	2.3123(19)	Ag(1)−N(2)	2.334(2)
Ag(1)−O(3)#2	2.502(2)	Ag(1)−O(2)	2.705(3)
N(1)−C(9)	1.291(3)	N(1)−Ag(1)#1	2.3123(19)
N(1)#1−Ag(1)−N(2)	128.95(7)	N(1)#1−Ag(1)−O(3)#2	115.05(7)
N(2)−Ag(1)−O(3)#2	115.67(7)	N(1)#1−Ag(1)−O(2)	81.35(7)
N(2)−Ag(1)−O(2)	113.58(7)	O(3)#2−Ag(1)−O(2)	79.09(7)

[a] Symmetry transformations used to generate equivalent atoms: (#1) $-x + 1, -y + 1, -z$; (#2) $-x + 2, -y + 1, -z$.

Table 8. Interatomic Distances (Å) and Bond Angles (deg) with Esd's in Parentheses for **6**[a]

Ag(1)−C(6)#1	2.287(8)	Ag(1)−N(1)	2.301(5)
Ag(1)−N(2)	2.303(5)	Ag(1)−C(5)#1	2.411(7)
Ag(1)−O(3)	2.515(5)		
C(6)#1−Ag(1)−N(1)	145.9(3)	C(6)#1−Ag(1)−N(2)	113.3(3)
N(1)−Ag(1)−N(2)	95.62(18)	C(6)#1−Ag(1)−C(5)#1	29.6(2)
N(1)−Ag(1)−C(5)#1	117.3(2)	N(2)−Ag(1)−C(5)#1	141.3(2)
C(6)#1−Ag(1)−O(3)	113.1(3)	N(1)−Ag(1)−O(3)	84.0(2)
N(2)−Ag(1)−O(3)	88.49(19)	C(5)#1−Ag(1)−O(3)	113.4(2)

[a] Symmetry transformations used to generate equivalent atoms: (#1) $-x + 1/2, -y + 3/2, -z$; (#2) $x, -y + 1, z$; (#3) $-x, y, -z$.

oxadiazole moiety basically lie in the same plane and are linked together at the *meta* position by the five-membered oxadiazole ring. **L9** and **L10** are soluble in common organic solvents such as CH_2Cl_2, $CHCl_3$, THF, CH_3OH, and C_2H_5OH, which facilitates the solution reaction between the ligands and inorganic metal salts. It is worthy pointing out that the coordination orientations of the terminal π-donors in **L9** and **L10** are different from that of heteratom donors in **L1**−**L8** (Scheme 1), which will results in the patterns of the coordination polymers based on **L9** and **L10** not easy

Table 9. Interatomic Distances (Å) and Bond Angles (deg) with Esd's in Parentheses for **7**[a]

Ag(1)−C(33)#1	2.324(3)	Ag(1)−N(3)	2.328(3)
Ag(1)−N(1)	2.335(3)	Ag(1)−C(32)#1	2.443(3)
Ag(1)−O(3)	2.519(3)	Ag(2)−N(4)	2.277(3)
Ag(2)−C(26)#2	2.288(4)	Ag(2)−N(2)	2.327(3)
Ag(2)−C(25)#2	2.451(3)	Ag(2)−O(3)	2.523(3)
C(33)#1−Ag(1)−N(3)	141.54(11)	C(33)#1−Ag(1)−N(1)	117.64(11)
N(3)−Ag(1)−N(1)	92.25(9)	C(33)#1−Ag(1)−C(32)#1	28.71(12)
N(3)−Ag(1)−C(32)#1	114.40(10)	N(1)−Ag(1)−C(32)#1	143.94(11)
C(33)#1−Ag(1)−O(3)	118.09(12)	N(3)−Ag(1)−O(3)	85.42(9)
N(1)−Ag(1)−O(3)	86.25(9)	C(32)#1−Ag(1)−O(3)	118.20(10)
N(4)−Ag(2)−C(26)#2	149.79(12)	N(4)−Ag(2)−N(2)	93.01(9)
C(26)#2−Ag(2)−N(2)	113.23(12)	N(4)−Ag(2)−C(25)#2	120.84(10)
C(26)#2−Ag(2)−C(25)#2	29.11(12)	N(2)−Ag(2)−C(25)#2	138.92(11)
N(4)−Ag(2)−O(3)	86.34(9)	C(26)#2−Ag(2)−O(3)	109.15(13)
N(2)−Ag(2)−O(3)	86.25(9)	C(25)#2−Ag(2)−O(3)	116.11(11)

[a] Symmetry transformations used to generate equivalent atoms: (#1) $-x$, $y + 1/2$, $-z + 1/2$; (#2) $-x$, $y - 1/2$, $-z + 1/2$.

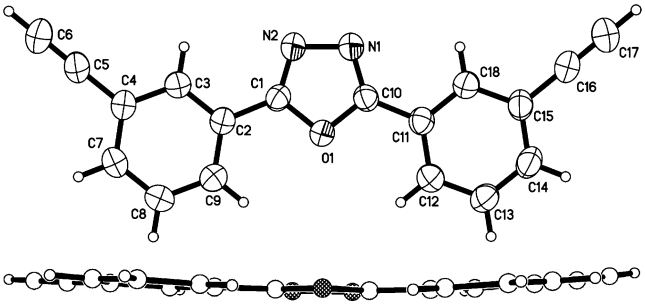

Figure 1. Molecular structure of **L10**.

achievable by the known bent organic spacers **L1**−**L8**. In addition, new ligands **L9** and **L10** give us a chance to modify them to new longer organic spacers with different coordination functional groups by some functional transform reactions related to −C≡CH, such as the well-known Heck−Cassar−Sonogashira−Hagihara reaction.[12]

Structural Analysis. Structural Analysis of $[Ag_2(\mathbf{L9})](SO_3CF_3)_2$ (1). Crystallization of **L9** with $AgSO_3CF_3$ in a CH_2Cl_2/C_6H_6 mixed solvent system at room temperature afforded the infinite two-dimensional chain structure in 87% yield. Single-crystal analysis revealed that there are two kinds of crystallographic Ag(I) centers in 1. Compound 1 is air stable. As shown in Figure 2, the first Ag(I) center lies in a $\{AgNO_3\pi\}$ coordination sphere, being made of one $N_{oxadiazole}$ donor (N(2), $d_{Ag(1)-N(2)} = 2.369(5)$ Å) and three O donors (O(2), O(6), and O(7), $d_{Ag(1)-O(2)} = 2.464(6)$, $d_{Ag(1)-O(6)} = 2.375(6)$, and $d_{Ag(1)-O(7)} = 2.525(5)$ Å) from one **L9** ligand and two coordinated $SO_3CF_3^-$ counterions and one π-donor (Ag(1)−C bond distances range from 2.532(5) to 2.753(5) Å) from the coordinated η^2-C≡CH group on the other **L9** ligand, respectively. It is worthwhile to point out that only one terminal −C≡CH group on **L9** involves the Ag(I) coordination sphere. Thus, the ligand **L9** herein acts as a tridentate ligand toward the Ag(I) ion. The second Ag(I) center adopts a $\{AgNO_4\}$ coordination sphere, consisting of one $N_{oxadiazole}$ donor (N(1), $d_{Ag(2)-N(1)} = 2.200(5)$ Å) and four $O_{triflate}$ donors from two coordinated triflate counterions. The

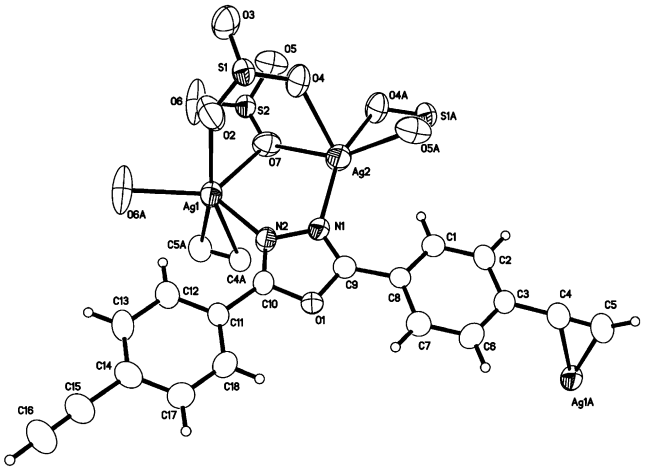

Figure 2. ORTEP figure of **1** (50% probability ellipsoids). Only coordinated oxygen atoms of triflate anions are shown.

Ag−O bond lengths range from 2.303 to 2.640 Å. Two Ag(I) atoms (Ag(1) and Ag(2)) are bridged by two $N_{oxadiazole}$ atoms and one triflate O-donor into a five-membered $\{Ag_2N_2O\}$ dinuclear core with a short Ag···Ag contact of 3.45 Å. The five-membered $\{Ag_2N_2O\}$ dinuclear core is different from the six-membered $\{Ag_2N_4\}$ moiety commonly found in many previous Ag(I)-coordination polymers based on **L1**−**L8**.[8]

In the solid state, Ag(I) atoms are bound to each other by coordinated triflate counterions into inorganic Ag(I)−$SO_3CF_3^-$ chains along the crystallographic *a* axis. The shortest intrachain Ag···Ag distance is 3.42 Å, which is slightly shorter than the sum of the van der Waals radii of two silver atoms, 3.44 Å (Figure 3).[13] These Ag(I)−$SO_3CF_3^-$ inorganic chains are separated by organic layers consisting of the **L9** ligands and, moreover, bound to the Ag(I)−$SO_3CF_3^-$ inorganic chains by Ag−N and Ag−π interactions into a two-dimensional network. As shown in Figure 4, the organic and inorganic layers are arranged alternatively along the crystallographic *b* axis in this two-dimensional net.

Structural Analysis of $[Ag(L9)]ClO_4$ (2). The **L9** ligand reacted with $AgClO_4$ in CH_2Cl_2/C_6H_6 at room temperature to produce the polymeric compound **2** as colorless crystals with novel one-dimensional network in 86% yield. Compound **2** is air stable. The structure of complex **2**, emphasizing the environment around the silver, is shown in Figure 5. Each Ag(I) center lies in a distorted tetrahedral coordination environment $\{AgN_2O\pi\}$ consisting of two oxadiazole N donors from two **L9** ligands (Ag(1)−N(1) = 2.257(5) and Ag(1)−N(2) = 2.295(5) Å), one coordinated ClO_4^- anion (Ag(1)−O(2) = 2.597(6) Å), and one terminal η^2-*C*≡*CH group (Ag(1)*−*C(5)* = *2.473(8) and Ag(1)*−*C(4)* = *2.768(8) Å). It is similar to compound **1***; only one −C≡CH group in **2** is coordinated to the silver center, and the Ag−π bonds serve as the interaction to link $\{Ag_2(\mathbf{L9})_2\}$ building blocks to form a one-dimensional polymeric chain along the crystallographic [101] direction (Figure 6).

As noted above, in complexes **1** and **2**, only one of two acetylene moieties of **L9** involves in the silver coordination

(12) (a) Dieck, H. A.; Heck, R. F. *J. Org. Chem.* **1975**, *40*, 259. (b) Cassar, I. *J. Org. Chem.* **1975**, *40*, 253. (c) Sonogashira, K.; Tohda, Y.; Hagihara, N. *Tetrahedron Lett.* **1975**, *16*, 4467.

(13) (a) Slater, J. C. *J. Chem. Phys.* **1964**, *41*, 3199. (b) Emsley, J. *The Elements*; Clarendon: Oxford, U.K., 1989; p 192.

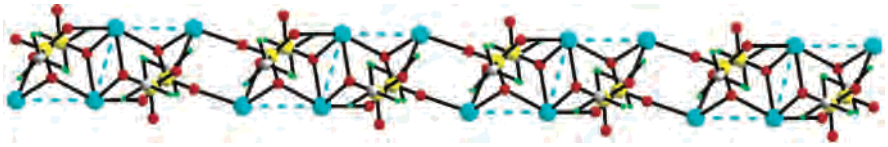

Figure 3. Ag(I)−$SO_3CF_3^-$ chain extended along the crystallographic *a* axis. The Ag···Ag interactions are shown as dotted lines.

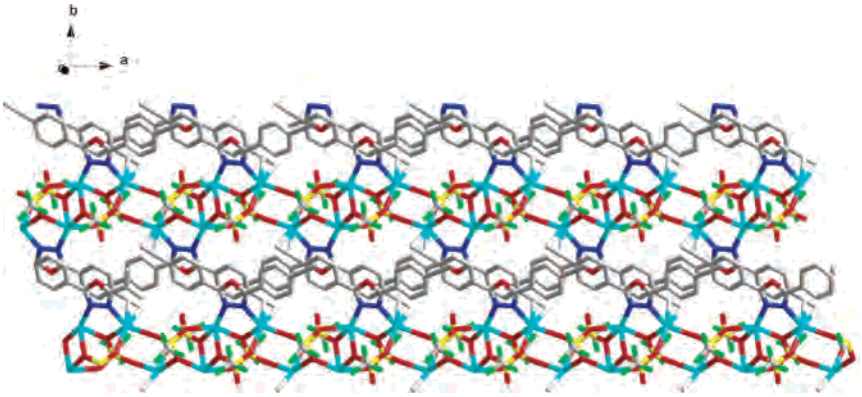

Figure 4. Crystal packing of **1**.

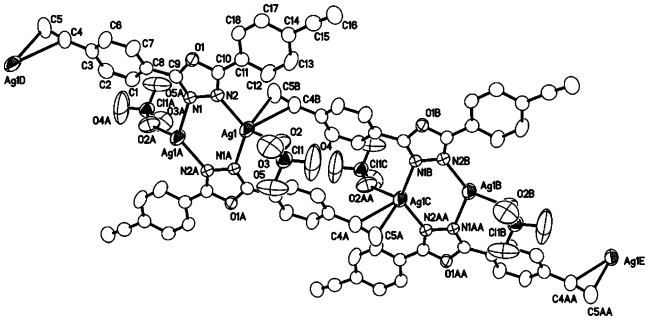

Figure 5. ORTEP figure of compound **2** (50% probability ellipsoids).

sphere and the other is free. However, it is worthy pointing out that, in these specific reactions, the final products do not depend on of the metal-to-ligand ratio. The different metal-to-ligand ratios including 1:2 and even 1:3 were tried in performing the reactions, and compounds **1** and **2** were isolated as the only products. The probably reason is that the O donor on the coordinated $SO_3CF_3^-$ or ClO_4^- preferentially involves the Ag(I) coordination sphere due to its stronger coordination tendency toward a "soft" Ag(I) atom than the weaker −C≡C− π donor.

Structural Analysis of [Ag(L9)]SbF_6 (3) and [Ag(L9)]-BF_4 (4). To investigate the effect of the counterion on the long-range order of the Ag(I)−**L9** coordination polymer, the weaker coordinated SbF_6^- and BF_4^- anions were used instead of the stronger coordination $SO_3CF_3^-$ and ClO_4^- anions.

Crystallization of **L9** with $AgSbF_6$ in a CH_2Cl_2/C_6H_6 mixed-solvent system at room temperature afforded the infinite noninterpenetrating two-dimensional polymeric compound **3** in 86% yield. Compound **3** is air stable. As shown in Figure 7, there is only one type of crystallographic Ag(I) center in **3**. It adopts a distorted tetrahedral $\{AgN_2\pi_2\}$ coordination sphere that consists of two $N_{oxadiazole}$ and two η^2-C≡CH groups from four **L9** ligands, respectively. In **3**, **L9** acts as a tetradentate ligand, in which two $N_{oxadiazole}$ and two η^2-C≡CH groups all involve the Ag(I) coordination sphere. The corresponding Ag(I)−$N_{oxadiazole}$ and

Ag(I)−C bonding distances are 2.281(7) and 2.555(14) Å, respectively. The Ag(I) and **L9** connectivity has the $\{Ag_2N_4\}$ groupings, which is different from the $\{Ag_2N_2O\}$ dinuclear core as observed in compound **1**. The Ag···Ag distance in the $\{Ag_2N_4\}$ moiety is 3.66 Å, which is slightly longer than the sum of the van der Waals radii of two silver atoms. It is different from **2**; the $\{Ag_2(\mathbf{L9})_2\}$ unit is introduced into a two-dimensional net by the Ag−π interactions (Figure 8) instead of a one-dimensional chain observed in **2**. This two-dimensional net is flat and contains the rhombuslike binuclear metallacycles. The crystallographic dimensions are 15 × 6 Å. In addition, these layers stack together exactly along the crystallographic *c* axis, and the uncoordinated SbF_6^- counterions are located between these layers (Figure 9).

Combination of $AgBF_4$ with **L9** in a CH_2Cl_2/benzene mixed-solvent system generates complex **4** at 87% yield. Compound **4** and **3** are isostructural. **4** crystallizes in the orthorhombic space group *Cmca*, which is the same as **3**. In **4**, the Ag(I) center lies in a distorted tetrahedral $\{AgN_2\pi_2\}$ coordination sphere which is analogous to that of **3** (Figure 10). In the solid state, compound **4** exhibits the same noninterpenetrating two-dimensional network (Figure 11) as found in compound **3**. Rhombuslike channels contain BF_4^- counterions. The corresponding channel dimensions are almost identical with those of **3**.

The common feature of compounds **3** and **4** lies that both terminal −C≡CH groups on the **L9** ligand coordinate to Ag(I) centers through a Ag−π interaction, which is distinctly different from the coordination behavior of **L9** in **1** and **2**. The only possible explanation for this change might be the coordination behaviors resulting from the different counterions (from coordinated anions $SO_3CF_3^-$ and ClO_4^- to uncoordinated SbF_6^- and BF_4^-) due to all three reactions

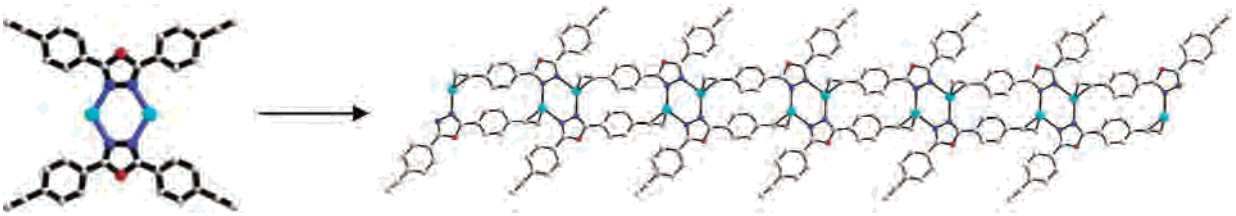

Figure 6. View of the one-dimensional chain architecture of **2**. The coordinated ClO_4^- anions are omitted for clarity.

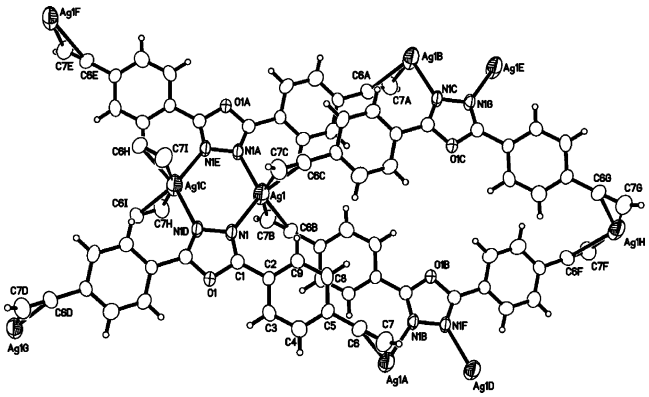

Figure 7. ORTEP figure of **3** (50% probability ellipsoids).

carried out under exactly the same conditions including solvent system, metal-to-ligand ratio, and temperature.

Structural Analysis of [Ag(L10)]SO_3CF_3 (5). The idea behind the use of ligand **L10** is to control supramolecular motifs through 3,3′-bibenzoacetylene-type lignds. It is well-known that the relative orientations of the coordination donors and also the different bridging spacing might result in unusual building blocks, which can lead to the construction of supramolecular motifs that have not been achieved using normal rigid linear organic ligands. Our previous studies demonstrated that five-membered 1,3,4-oxadiazole-bridged 3,3′-bipyridine and 3,3′-biphenylamine ligands could bind metal ions by cis or trans conformation and result in a framework topology that is versatile, sometimes even in affecting the formation of polymer vs molecule. The immediate coordination arrangement around the silver center in **5** is shown in Figure 12. Each silver center in **5** lies in a distorted tetrahedral $\{AgN_2O\pi\}$ coordination sphere, with two oxadiazole N donors from two **L10** ligands, one O donor from the one coordinated $SO_3CF_3^-$ counterion, and a pair of π-electrons from the coordinated η^1-C≡CH group from the third **L10** ligand. The Ag−C(6) bond distance is 2.855(16) Å, while the Ag···C(5) contact is 3.149(15) Å, which is much longer than the normal Ag−C bond length of 2.80 Å. The Ag−N bond distances are 2.3123(19) and 2.334(2) Å, respectively, which are comparable to the corresponding bond lengths of **1**−**4**. The Ag−O bond length is 2.502(2) Å, which lies in the normal range of Ag−O bond distance. Herein, only one of two terminal −C≡CH groups of **L10** coordinates to the Ag(I) center, which is the same as observed in compounds **1** and **2**. Two Ag(I) atoms are connected by two **L10** ligands through the four oxadiazole N donors to form an "X-shaped" building block, in which two **L10** ligands are exactly in the same plane. The Ag··· Ag distance is 3.41 Å, which is slightly shorter than the than the sum of the van der Waals radii of two silver atoms, 3.44 Å.

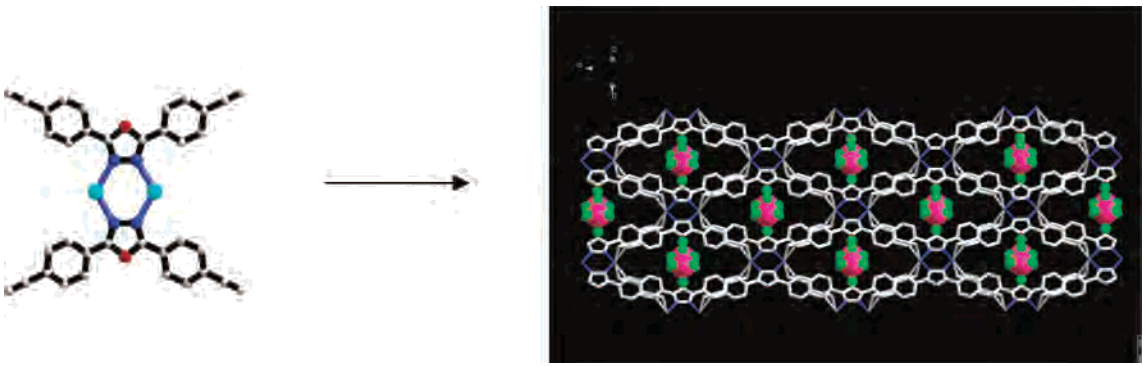

Figure 8. $Ag_2(\mathbf{L9})_2$ building blocks bound together by Ag−π interactions into a two-dimensional net in **3**.

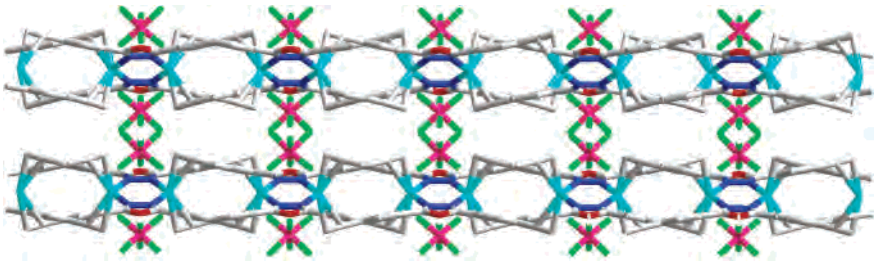

Figure 9. Side view of two layers in **3**.

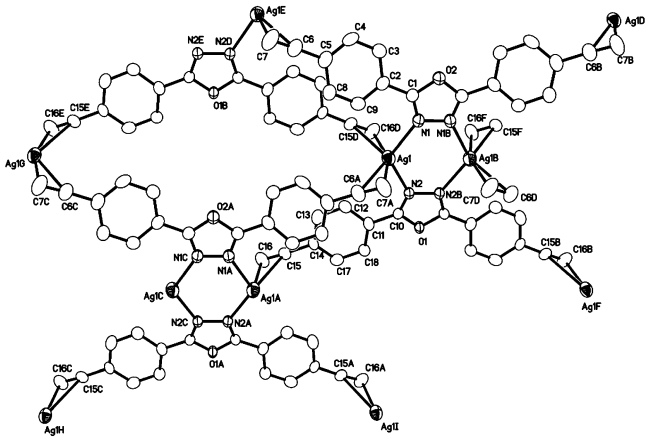

Figure 10. ORTEP figure of **4** (50% probability ellipsoids).

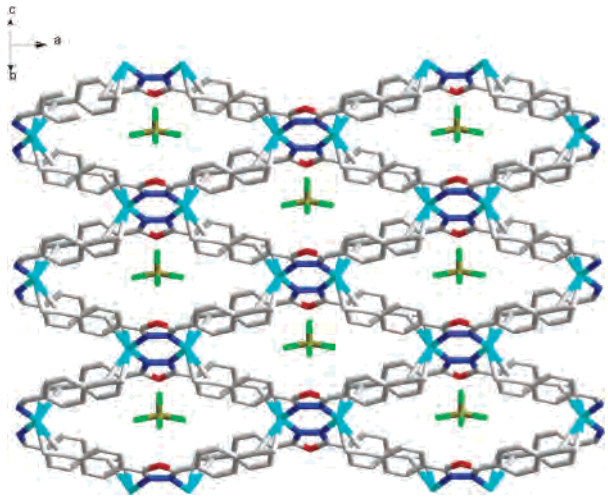

Figure 11. Two-dimensional net in **4**. Uncoordinated BF_4^- counterions are located in the channels.

The architectural pattern of **5** demonstrates a one-dimensional chain motif composed of the $\{Ag_2(\mathbf{L10})_2\}$ "X-shaped" moieties linked via the two crystallographic equivalent Ag$-\pi$ bonds (Figure 13). These chains extend along the crystallographic *c* axis and, moreover, stack together in a face-to-face fashion through a weak interchain $\pi-\pi$ interaction (3.5 Å) along the crystallographic *b* axis (Figure 14) to generate a three-dimensional network containing almost regular honeycomblike channels being filled with coordinated $SO_3CF_3^-$ counterions (Figure 15). The effective cavity size of the channel is ca. 6 × 8 Å. The shortest interchain Ag···Ag separation is 5.9 Å.

The assembly of a honeycomblike is challenging since the hexagon represents the one of the most common motifs in nature.[14] However, synthetic noninterpenetrating three-dimensional networks with honeycomblike cross sections are still unusual, although some two-dimensional honeycomblike nets, such as $[Ni(BTC)]_3[BTC]_2\cdot 14H_2O\cdot 2C_5H_5N$ (BTC = 1, 3, 5-benzenetricarboxylate) and [Ag(TCB)(CF_3SO_3)] (TCB = 1, 3, 5-tricyanobenzene),[16] have been previously obtained. In the solid state, these two-dimensional nets stack in parallel and generate honeycomblike channels. An interesting three-dimensional network, namely ZnF(3-amino-1,2,4-triazole), was reported very recently.[15e] Similar regular honeycomblike channels have been found. The channels have a 12 × 12 Å dimension that is larger than that of in **5**. To our knowledge, compound **5** reported herein is the first example of a non-interpenetrating three-dimensional honeycomblike channel-containing network formed by one-dimensional chains through interchain $\pi-\pi$ interactions. Compared to **1**, the polymeric pattern changes from a two-dimensional net in **1** to a $\pi-\pi$ interaction driven three-dimensional framework in **5**, indicating of the remarkable influence of the different orientations of the −C≡CH donors on the phenyl rings.

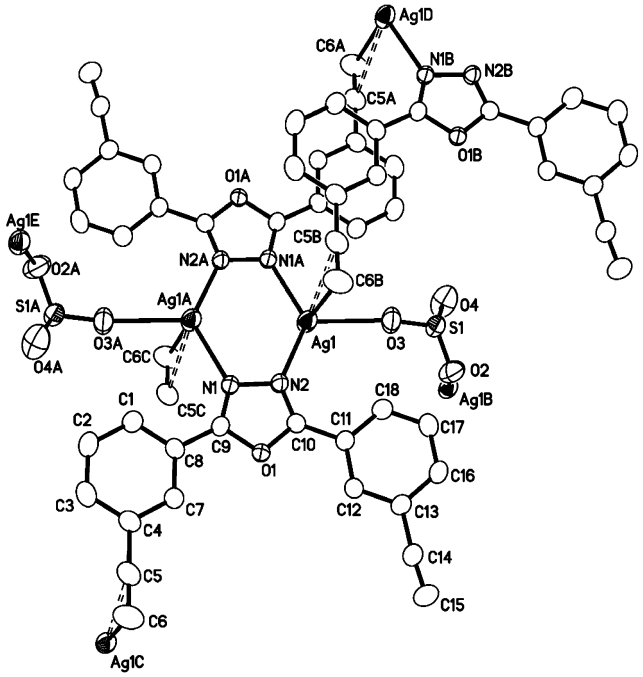

Figure 12. ORTEP figure of **5** (50% probability ellipsoids).

Structural Analysis of $[Ag(L10)(H_2O)_{0.5}]BF_4\cdot 0.5H_2O$ (6). To explore the effect of the counterion on the long-range order of the Ag(I)−**L10** coordination polymer, the weakly coordinating BF_4^- anion was used instead of the more strongly coordinating $SO_3CF_3^-$ anion. Crystallization of **L10** with $AgBF_4$ in the same mixed solvent system at room temperature afforded polymeric compound **6** in 85% yield. Compound **6** is air stable. Single-crystal X-ray analysis of compound **6** showed that the silver atom resides in a distorted $\{AgN_2O\pi\}$ tetrahedral coordination environment, consisting of two oxadiazole N donors (Ag(1)−N(1) = 2.301(5) and Ag(1)−N(2) = 2.303(5) Å), one O donor (Ag(1)−O(3) = 2.515(5) Å) from a coordinated water molecule, and one pair of π electrons from one η^2-C≡CH group (Ag(1)−C(6) = 2.287(8) and Ag(1)−C(5) = 2.411(7) Å). It is worth pointing

(14) Ozin, G. A. *Acc. Chem. Res.* **1997**, *30*, 17.

(15) (a) Choi, H. J.; Suh, M. P. *J. Am. Chem. Soc.* **1998**, *120*, 10622. (b) Gardner, G. B.; Venkataraman, D.; Moore, J. S.; Lee, S. *Nature* **1995**, *374*, 792. (c) Abrahams, B. F.; Hoskins, B. F.; Liu, J.; Robson, R. *J. Am. Chem. Soc.* **1991**, *113*, 3045. (d) Abrahams, B. F.; Hoskins, B. F.; Robson, R. *J. Chem. Soc., Chem. Commun.* **1990**, 60. (e) Su, C.-Y.; Goforth, A. M.; Smith, M. D.; Pellechia, P. J.; zur Loye, H.-C. *J. Am. Chem. Soc.* **2004**, *126*, 3576.

(16) The pore dimensions described here are crystallographic scalar quantities and do not account for the van der Waals radii of the atoms defining the pore.

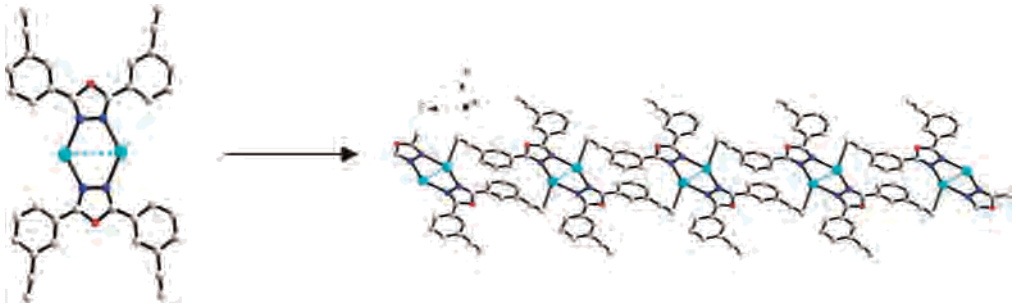

Figure 13. "X-shaped" building block for a one-dimensional chain in **5**. The Ag···Ag distances are shown as dotted lines.

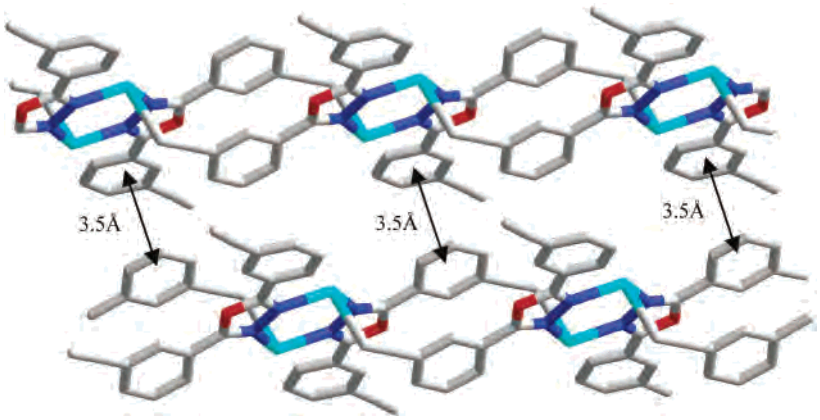

Figure 14. Two sets of one-dimensional chains stacking together through interchain $\pi-\pi$ interactions.

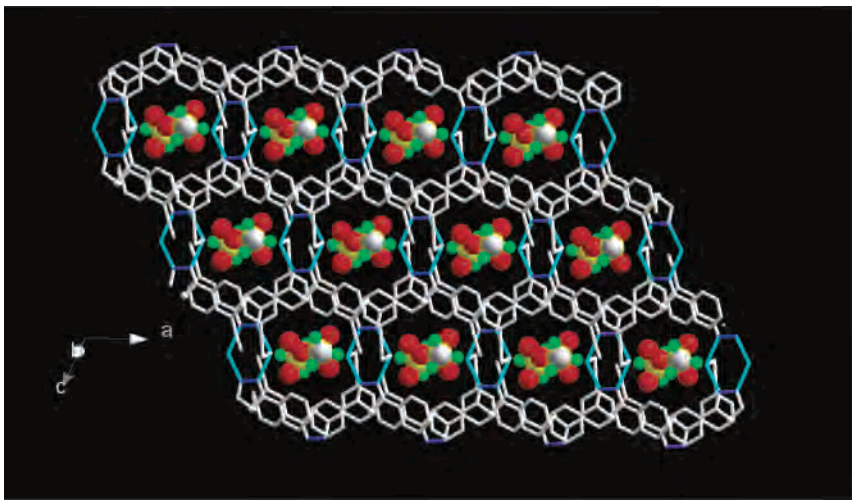

Figure 15. View of the honeycomblike channel-containing three-dimensional structure in **5**. $SO_3CF_3^-$ anions are located in channels.

out that there are two independent **L10** ligands in **6**. The first type of **L10** ligand acts as a tetradentate coordination spacer, whereas the second one displays a bidentate ligand (Figure 16). Two silver atoms are connected to each other by four oxadiazole N donors from the first and second types of **L10** ligand, respectively, giving rise to a $\{Ag_2(\mathbf{L10})_2\}$ moiety, in which these two silver atoms are bridged together by a coordinated water molecule.

In the solid state, two sets of $\{Ag_2(\mathbf{L10})_2O\}$ building blocks rightabout orientate and are linked by two sets of terminal Ag$-\pi$ bonds to form a one-dimensional zigzag chain running along the crystallographic *b* axis (Figure 17). The uncoordinated BF_4^- anions are located between these zigzag chains and bound to them by four sets of interchain F···H−C hydrogen bonds. Every two sets of H-bonds extend along the crystallographic *a* and *c* axes (Figure 18), respectively. The F(5)···H(6) and F(6)···H(17) distances are 2.394(5) and 2.632(6) Å, respectively. The corresponding F(5)···C(6) and F(6)···C(17) distances are 3.14(5) and 3.21(4) Å, respectively, and the corresponding F(5)···H(6)−C(6) and F(6)···H(17)−C(17) angles are 132.58(5) and 123.98(4)°, respectively. As shown in Figure 19, one-dimensional zigzag chains are linked together by these four sets of F···H−C bonds to generate a novel noninterpenetrating three-dimensional H-bonded framework (Figure 19). The three-dimensional framework consists of two different kinds of channels, i.e., big ellipse-like and rectangle-like channels, extending along the crystallographic *c* axis. The crystal-

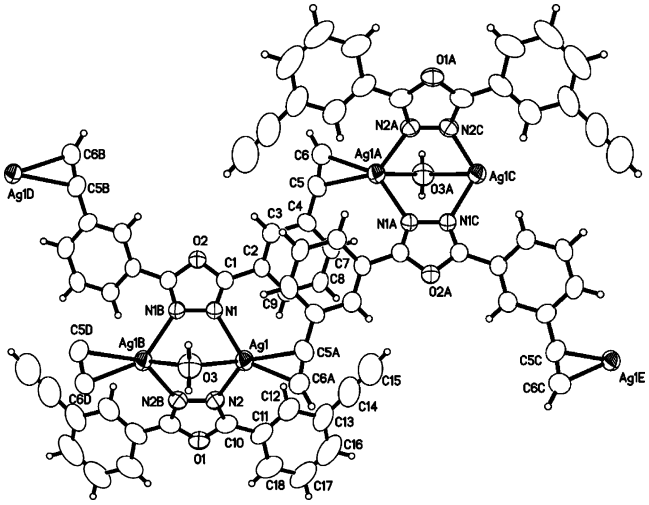

Figure 16. ORTEP figure of **6** (50% probability ellipsoids).

lographic dimensions[16] are 15.17 × 9.31 and 5.91 × 4.26 Å, respectively. The large ellipse-like channels are guest free, while the small rectangle-like channels are filled with water guest molecules and hydrogen bonded to the framework through the weak F···H−O hydrogen bonds (Figure 20). The corresponding F···H, F···O, and −F···H−O data are 2.62(3) and 3.02(3) Å and 111.98(5)°, respectively. The existence and structural importance of weak C−H···X hydrogen-bonding interactions are now well established[17] and are observed in many compounds, such as the N···H−C interaction in 1,3,5-tricyanobenzene−hexamethylbenzene,[18a] the O···H−C interaction in $(C_{14}H_{12}N_2)[Cu(opba)]\cdot 3H_2O$ and $Na_2(C_{12}H_{12}N_2)[Cu(opba)]_2\cdot 4H_2O$ (opba = *o*-phenylenebis(oxamate)),[18a] and the F···H−C interaction in 11-(trifluoromethyl)-15,16-dihydrocyclopenta[α]phenanthren-17-one.[19] These hydrogen bonds, although weak, contribute significantly to the structural organization of **6** in the crystalline state.

Structural Analysis of $\{[Ag_2(L10)_2(H_2O)]ClO_4\}\cdot$(*o*-xylene) (7). To investigate the templating effect of the solvent and counterion on the long-range order of the Ag(I)−**L10** coordination polymer, xylene and ClO_4^- were used instead of benzene and BF_4^- to perform the reaction. When a solution of **L10** in methylene chloride was treated with $AgClO_4$ in xylene, using a metal-to-ligand ratio of 1:1, compound **7** was obtained as colorless crystals in 85% yield. Single-crystal X-ray analysis revealed that there are two crystallographic independent Ag(I) atoms in **7**, and they are all located in a distorted $\{AgN_2O\pi\}$ coordination sphere. As shown in Figure 21, the coordination environment of each silver atom is defined by two $N_{oxadiazole}$ donors from two **L10** ligands, one O donor from a coordinated water molecule, and a π-donor from a −C≡CH moiety. For Ag(1) and Ag(2) centers, the Ag−N and Ag−O bond lengths lie in a range of 2.277(3)−2.335(3) and 2.519(3)−2.523(3) Å, respectively. The Ag−C bond distances are in the range of 2.288(4)−2.451(3) Å. All the bond distances herein are similar to those corresponding bond lengths of **6**. Compared to **6**, the same one-dimensional zigzag chain consisting of the same $\{Ag_2(\mathbf{L10})_2O\}$ building blocks has been found (Figure 22). It is worthy to point out that the hydrogen-bonding system in **7** is different from that of **6**. As shown in Figure 23, one-dimensional zigzag chains are linked together by two sets of equivalent O−H···O hydrogen bonds along the crystallographic *c* axis into a two-dimensional net. The corresponding O···H, O···O, and −O···H−O data are 2.62(3) and 3.02(3) Å and 111.98(5)°, respectively. In addition, O···H−C hydrogen-bonding interactions are present in **3**, too. As shown in Figure 24, the O···H−C hydrogen-bonding system along the crystallographic *c* axis involves O(11) and O(10) of the ClO_4^- anions and H(3) and H(33) on the phenyl and acetylene groups of **L10** ligand of the neighboring chains (O(10)···H(3), C(3)···O(10), and −O(10)···H(3)−C(3) are 2.49(3) and 3.30(3) Å and 147.23(5)°, respectively; O(11)···H(33), C(33)···O(11), and −O(11)···H(33)−C(33) are 2.53(3) and 3.19(3) Å and 128.26(5)°, respectively). The O···H−C hydrogen-bonding system along the crystallographic *a* axis

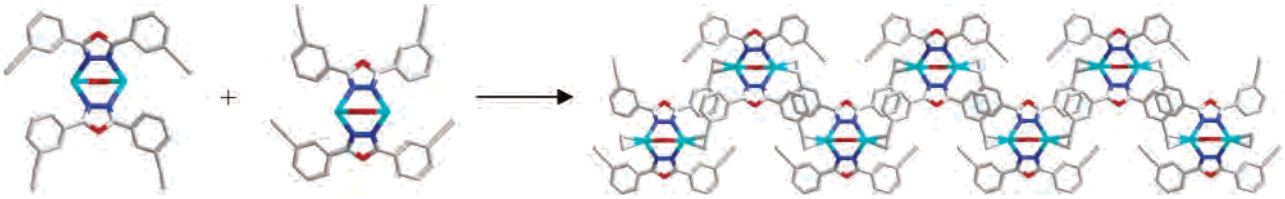

Figure 17. Two sets of conversely orientated $\{Ag_2(\mathbf{L10})_2O\}$ building blocks being linked by Ag−π bonds into a one-dimensional zigzag chain.

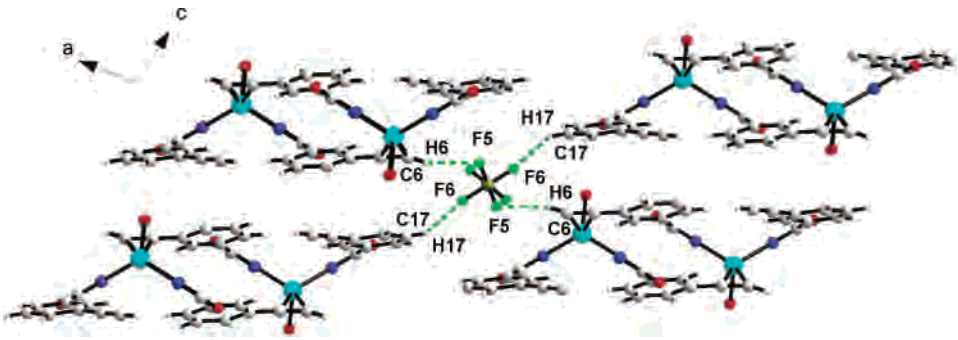

Figure 18. Interchain F···H−C hydrogen-bonding systems. The view is shown down the crystallographic *b* axis.

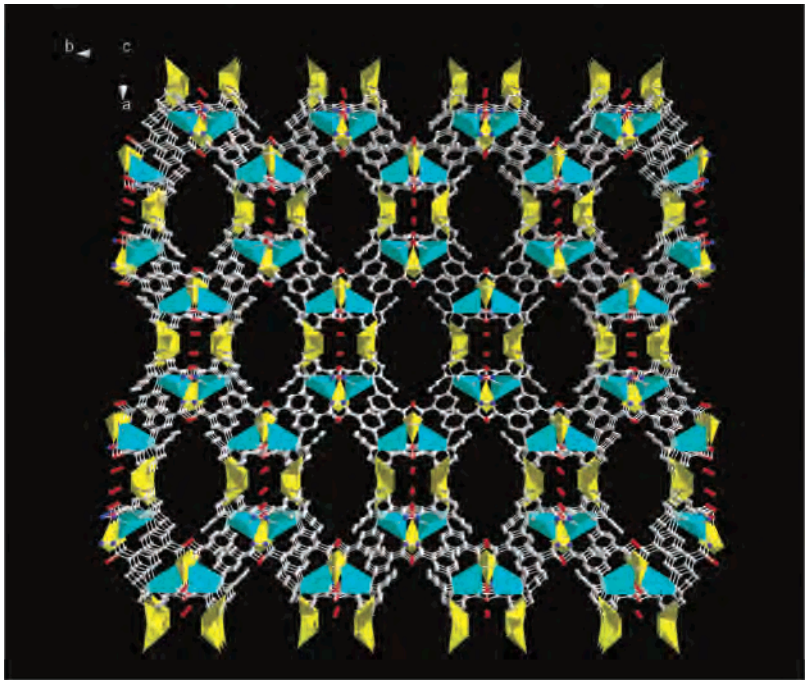

Figure 19. H-bonded three-dimensional framework of **6**.

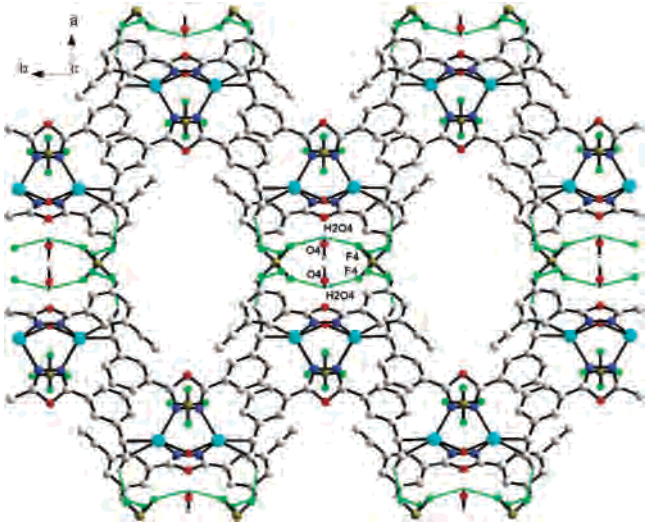

Figure 20. Guest water molecules located in the small rectangle-like channels and fixed by F···H−O hydrogen bonds.

consists of O(4) and O(6) of the ClO_4^- anions and H(21) and H(23) on the phenyl groups of **L10** ligand of the adjacent chains (O(4)···H(21), C(21)···O(4), and −O(4)···H(21)−C(21) are 2.57(3) and 3.23(3) Å and 128.65(5)°, respectively; O(6)···H(23), C(23)···O(6), and −O(6)···H(23)−C(23) are 2.59(3) and 3.50(3) Å and 168.37(5)°, respectively). Thus, the strong O−H···O and weak O−H···C hydrogen bonds serve as the glue to link one-dimensional chains into a three-dimensional hydrogen-bonded infinite structure. As shown in Figure 25, the noninterpenetrating three-dimensional network with rhombic channels (effective cross-section of ca. 14 × 13 Å) extends along the crystallographic *a* axis, in which the *o*-xylene molecules are located as the guest. It is interesting that compound **7** exhibits a significant affinity to

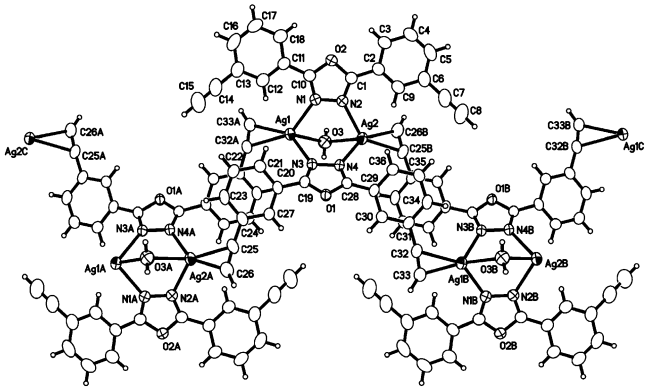

Figure 21. ORTEP structure of **7** (50% probability ellipsoids).

o-xylene molecules. As shown herein, only *o*-xylene molecules other than *m*- and *p*-xylol molecules have been clathrated during the crystallization in xylene of **7**. The ^{1}H NMR (DMSO-d_6) of **7** showed a single peak at 2.19 ppm and the multiple peaks in the range of 7.02−7.18 ppm, which was attributed to the proton on the clathrated *o*-xylene molecules. This could be an additional evidence for this novel crystallized process. Such crystallization of **7** in xylene could be considered as shape-selective process,[20] and compound **7** might find potential applications such as xylene isomers purification. Further studies are needed to elucidate the mechanism why compound **7** can selectively clathrate *o*-xylene but not *m*- and *p*-xylol. A systematic investigation is underway on the inclusion properties and guest exchange

(17) Desiraju, G. R. *Acc. Chem. Res.* **1996**, *29*, 441.

(18) (a) Reddy, D. S.; Goud, B. S.; Panneerselvam, K.; Desiraju, G. R. *J. Chem. Soc. Commun.* **1993**, 663. (b) Unamuno, I.; Gutiérrez-Zorrilla, J. M.; Luque, A.; Román, P.; Lezama, L.; Calvo, R.; Rojo, T. *Inorg. Chem.* **1998**, *37*, 6452.

(19) Sano, Y.; Tanaka, M.; Koga, N.; Matsuda, K.; Iwamura, H.; Rabu, P.; Drillon, M. *J. Am. Chem. Soc.* **1997**, *119*, 8246.

(20) (a) Kosal, M. E.; Chou, J.-H.; Wilson, S. R.; Suslick, K. *Nature* **2002**, *1*, 121. (b) Fujita, M.; Kwon, Y. J.; Washizu, S.; Ogura, K. *J. Am. Chem. Soc.* **1994**, *116*, 1151.

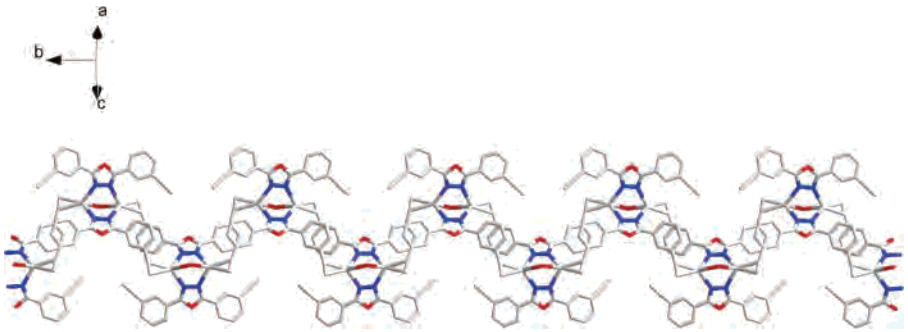

Figure 22. One-dimensional zigzag chain composed of $\{Ag_2(\mathbf{L10})_2O\}$ building block in **7**.

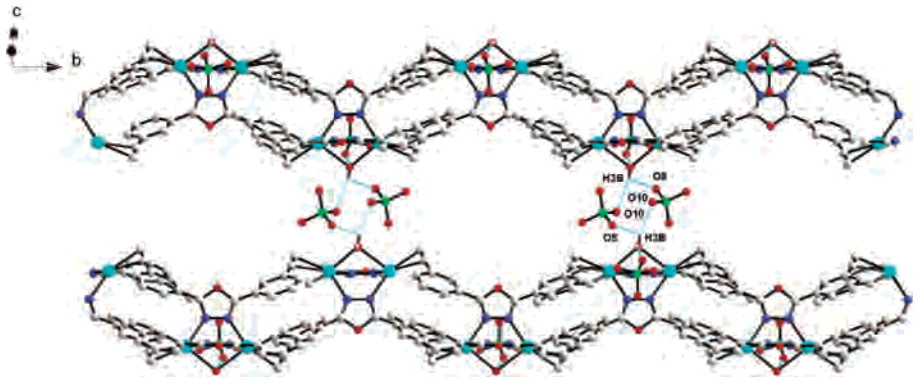

Figure 23. One-dimensional chains of **7** connected to each other by two sets of equivalent O−H···O hydrogen bonds.

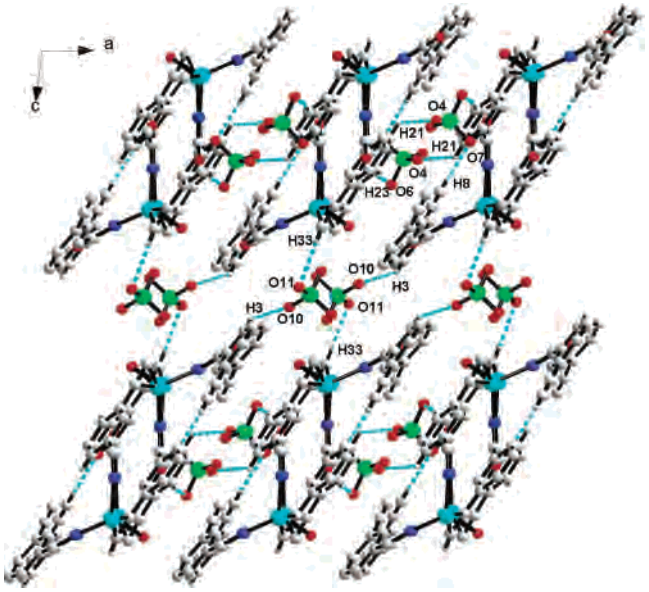

Figure 24. O···H−C hydrogen-bonding systems cross-linking the one-dimensional chains extending along the crystallographic *a* and *c* axes.

of **7**. Thermogravimetric analyses traces of **7** (Figure 26) show a weight loss of 1.66% from 50 to 90 °C corresponding to the loss of the water molecules (calcd 1.67%). A second weight loss of 9.6% from 140 to 229 °C corresponds to removal of the guest *o*-xylene molecules (calculated 9.8%). The third weight loss, observed from 250 to 392 °C, corresponds to the release of the one of the two ligands of **L10** (obsd 24.5%, calcd 25.0%). The forth weight loss (obsd 24.1%, calcd 25.0%) above 400 °C corresponds to the release of the remaining **L10** ligand. ^{1}H NMR spectra of **7** show that all *o*-xylene guest molecules could be removed at ∼200 °C (Figure 27), which is consistent with the results of TGA. The X-ray powder diffraction (XRD) pattern of thermally desolvated sample of **7** is compared with that of as-synthesized, solvent-containing **7** in Figure 28. The XRD pattern after heating show that the shapes and intensities of some reflections are slightly changed relative to that of the original sample. This indicates that the porous framework of **7** is maintained after the guest removal.

IR, ^{1}H NMR, and UV/Vis Spectra. The IR spectra of all complexes display the characteristic strong $\nu_{C\equiv C-H}$ band around 3280 cm^{-1}, corroborating the −C≡CH being the terminal functional group in **L9** and **L10**. IR spectra of complexes **3** and **4** reveal weak $\nu_{C\equiv C}$ vibrations of the coordinated −C≡CH groups at 2072−2109 cm^{-1}, which is shifted by ∼98 cm^{-1} to lower energy compared to the free alkynes (2169−2170 cm^{-1}). The IR of **1** and **2** and **5**−**7** show two bands in the C≡C stretching region at 2169−2170 and 2072−2109 cm^{-1}, respectively. The bands in the region of 2169−2170 cm^{-1} correspond to the uncoordinated −C≡CH groups, while the bands in the region of 2072−2109 cm^{-1} correspond to the coordinated −C≡CH groups. Such a shift of $\nu_{C\equiv C}$ upon η^2-coordination in complexes **1**−**7** is similar to what is generally observed for alkynes being two-electron π-donors to the Ag(I) center.[21]

Compounds **1**−**7** are insoluble in common organic solvents due to their polymeric nature. They are soluble in CH_3CN and slightly soluble in DMSO and DMF. The ^{1}H NMR and UV/vis spectra of complexes **1**−**7** in solution are identical with those of the free ligands, which indicates all complexes

(21) (a) Lin, Y.-Y.; Lai, S.-W.; Che, C.-M.; Cheung, K.-K.; Zhou, Z.-Y. *Organometallics* **2002**, *21*, 2275. (b) Chui, S. S. Y.; Ng, M. F. Y.; Che, C.-M. *Chem.*—Eur. J. **2005**, *11*, 1739.

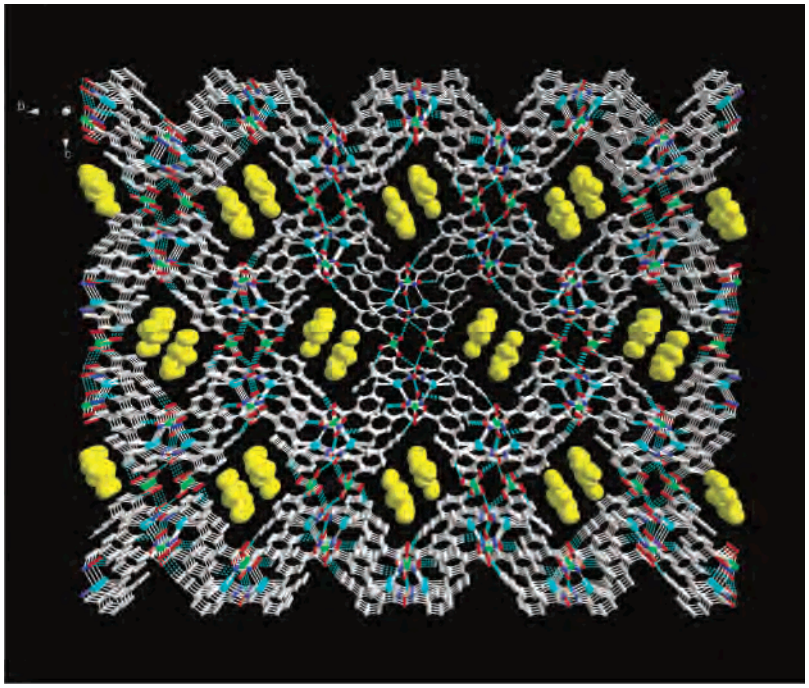

Figure 25. H-bonded three-dimensional network of **7**. *o*-Xylene guest molecules (shown as space-filling) are located in the rhombic channels.

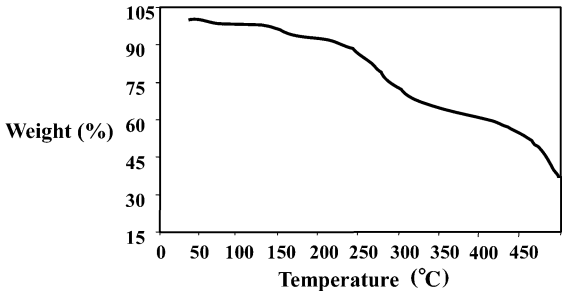

Figure 26. TGA trace of **7**.

were dissolved to dissociate into oligomers or the starting materials in solution.

Theoretical Calculations. To gain a deeper insight into the coordination behavior of this type of ligands, we performed ab initio Mulliken population analysis on ligands **L9** and **L10**.[22] For this study, DFT calculations with the B3LYP functional and the 6-31G(d) basis set were used. Full geometry optimizations without any symmetry constraints were carried out. Harmonic frequencies were also calculated at the optimized structure at the same level of accuracy, and no imaginary frequency was found to confirm the resulting structure is a minimum. The calculations were performed with the Gaussian 98 software on a Pentium computer. The calculated results of **L9** show that the values of total atomic charges for two terminal carbon atoms are negative (−0.5971), which indicates the strong coordination tendency toward to soft silver atom. As expected, the total atomic charges of two nitrogen (−0.3497) and one oxygen (−0.4913) atoms on central oxadiazole ring are negative too, which is usual for electronegative heteroatoms.

(22) (a) Bianco, A,; Bertarelli, C.; Rabolt, J. F.; Zerbi, G. *Chem. Mater.* **2005**, *17*, 869. (b)Nandina, G.; Sathyanarayana, D. N. *J. Mol. Struct. (THEOCHEM)* **2002**, *579*, 1.

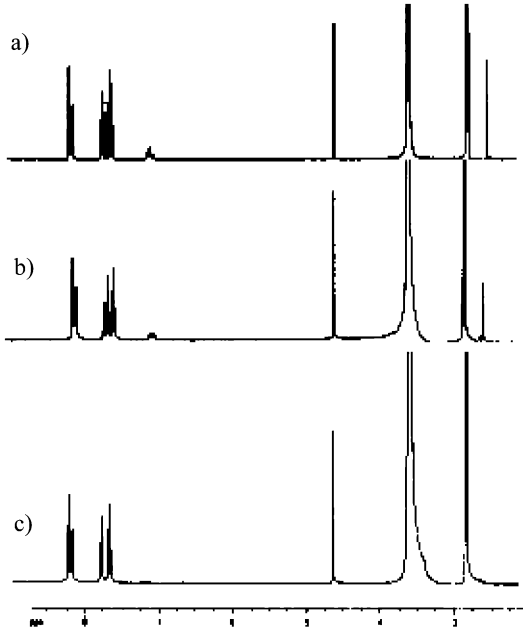

Figure 27. ^{1}H NMR spectra of **7** in DMSO-d_6. (a) ^{1}H NMR spectrum of original sample of **7** recorded at room temperature is shown. (b) The solid sample of **7** was heated to 90 °C and then dissolved in DMSO-d_6, and the spectrum was recorded at ambient temperature. (c) The solid sample of **7** was heated to 200 °C and then dissolved in DMSO-d_6, and the spectrum was recorded at ambient temperature.

L10 is different from **L9**. The calculation results of **L10** show that the energies of three possible conformations of **L10** in either gas or benzene solution are almost identical (Table 10). Thus, these three conformations I−III could be concomitant in gas or benzene solution (Chart 2). As shown above, **L10** adopts conformation I to bind the Ag(I) atom in **5**, while it adopts both conformations I and III to bind Ag(I) atoms in compounds **6** and **7**. However, no conformation II was found in compounds **5**−**7**. **L10** is similar to **L9** in that the atomic charges of the terminal carbon atoms and two

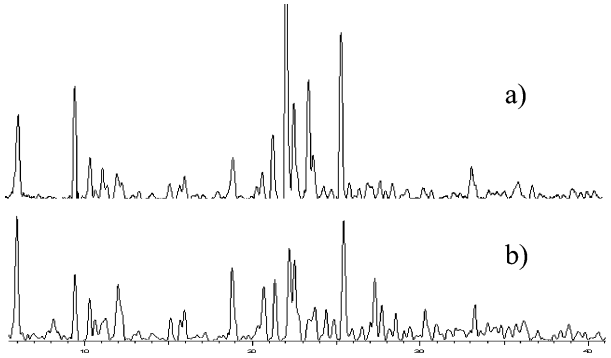

Figure 28. X-ray powder diffraction patterns of **7**: (a) original crystals of **7**; (b) **7** heated to 200 °C.

nitrogen and one oxygen atoms on central oxadiazole ring of **L10** are negative (Table 10), which provide a supportive trend for the current results and discussion.

Electrical Conductivity. Synthesis of single-component molecular coordination complexes by the judicious choice of organic spacers and metal centers can be an efficient method for obtaining new types of conductive materials,[23] for example, $[M(dimt)_2]_2$-type molecular complexes (M = Ni(II), Pd(II), Pt(II), Cu(II), and so on; dimt = 4,5-dimercapto-1,3-dithiole-2-thione).[24] Some of them have been confirmed to be semiconductors or superconductors. Up to date, a number of molecular-based transition metal complexes with interesting electrical conductivity have been reported. However, the study of conductive properties on polymeric coordination complexes has received considerably less attention. To explore the electrical conductive properties of these new polymeric complexes, the electrical conductive experiment were performed on compounds **2, 5**, and **7** in the solid state. The conductivity measurements of **2**, **5**, and **7** were performed on single crystals at a direction on the *ac* plane for **2** and *ab* plane for **5** and **7**, respectively. The single crystal was fixed between a gold plate (10 × 4 × 1 mm) and thin gold wire (0.2 mm in diameter which is smaller than those of single crystals) on the piece of organic glass using gold paste. Two gold wires extended from these two electrodes were connected to an Agilent Technologies 4294A-ATO-20150. The scan range of 5 ± 0.1 MHz was chosen during the measurement. The conductance (G) and susceptance (B) values were obtained totally on the basis of 401 scanning dots. The resistivity (ρ) of the complexes was obtained depending on the formula of $S/(LG)$ ($S = \pi r^2$, L = length of the single crystals). The dielectric constant (ϵ_r) of complexes was obtained depending on the formula of $BL/(2\pi fs)$. The primary result indicates that metal−organic complexes **2**, **5**, and **7** behave as typical semiconductors with a resistivity (ρ) value lying in the range of 0.302×10^2−2.926×10^2 Ω·m (Table 11). The corresponding dielectric constants (ϵ_r) of **2**, **5**, and **7** were obtained in the range of 12.4×10^2−148.3×10^2.

Luminescent Properties of L9, L10, and 1−7. Inorganic−organic hybrid coordination polymers have been investigated for fluorescence properties and for potential applications as luminescent materials, such as light-emitting diodes (LEDs).[25] Owing to the higher thermal stability of inorganic−organic coordination polymers and the ability of affecting the emission wavelength of organic materials, syntheses of inorganic−organic coordination polymers by the judicious choice of conjugated organic spacers and transition metal centers can be an efficient method for obtaining new types of electroluminescent materials, especially for d^{10} or d^{10}−d^{10} systems[26] and oxadiazole-containing complexes.[27] We have been exploring the luminescent properties of **L1**−**L8** and organic−inorganic coordination polymers and supramolecular complexes based on them in the solid state. The results indicate that emission colors of organic spacers **L1**−**L8** were affected by their incorporation into metal-containing coordination compounds. The luminescent properties of **L9**

Table 10. Calculation Results for **L10**[a]

	isomer I state		isomer II state		isomer III state	
param	gas	C_6H_6	gas	C_6H_6	gas	C_6H_6
energy (au)	−876.2715	−876.2721	−876.2718	−876.2723	−876.2721	−876.2725
dipole moment	3.9620	4.4311	3.3885	3.8667	2.7998	3.2558
charges						
atom N1	−0.2808	−0.2843	−0.2839	−0.2870	−0.2841	−0.2870
atom N2	−0.2808	−0.2843	−0.2811	−0.2842	−0.2841	−0.2870
atom O3	−0.5117	−0.5102	−0.5100	−0.5087	−0.5079	−0.5069
atom C4	0.0613	0.0635	0.0577	0.0546	0.0578	0.0552
atom C5	−0.5066	−0.5102	−0.5097	−0.5040	−0.5089	−0.5044
atom C6	0.0613	0.0635	0.0614	0.0634	0.0578	0.0552
atom C7	−0.5066	−0.5102	−0.5070	−0.5105	−0.5089	−0.5044

[a] Dielectric constant of benzene solution: 2.247. Solute radii: (I) 5.19 Å; (II) 5.23 Å; (III) 5.15 Å

Chart 2. Possible Conformations I−III of **L10**

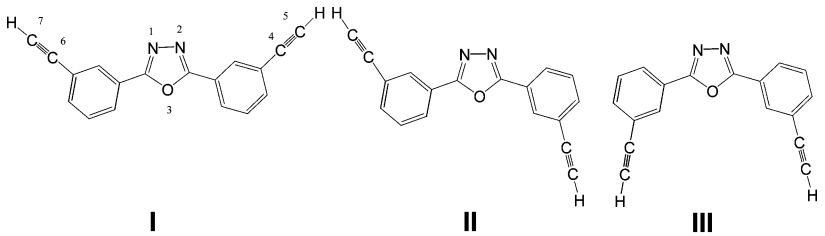

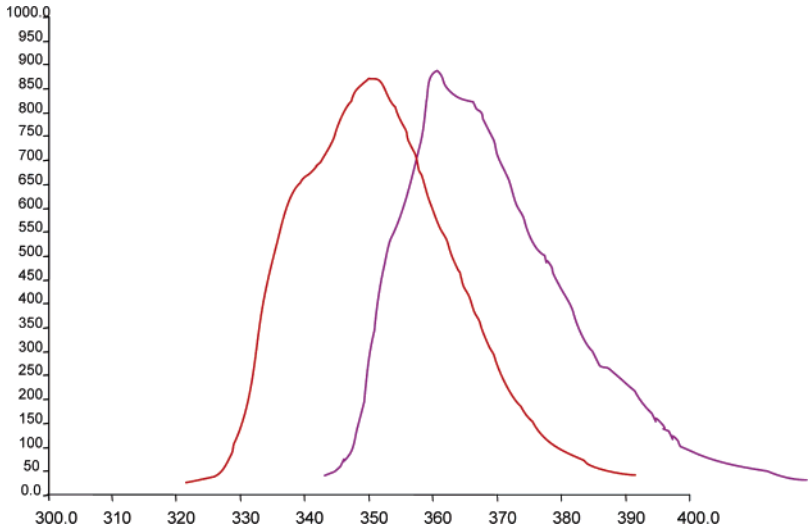

Figure 29. Photoinduced emission spectra of **L9** (red) and **L10** (purple) in CH_3CN.

Table 11. $\lambda_{ex}/\lambda_{em}$ (nm) Luminescent Properties of **L9**, **L10**, and **1**−**7** in the Solid State and CH_3CN

compd	solid state	CH_3CN	compd	solid state	CH_3CN
L9	203/387	205/361	**4**	202/425	211/360
L10	204/386	202/350	**5**	202/395	203/348
1	202/424	207/358	**6**	204/397	211/347
2	202/422	207/357	**7**	202/397	202/357
3	202/423	206/356			

Table 12. Electrical Conductivity of Compounds **2**, **5**, and **7**[a]

compd	L (μm)	G (ns)	B (μs)	r (10^{-5} Ω^{-1}·cm^{-1})	$10^{-2}\rho$ (Ω·m)	$10^{-2}\epsilon_r$
2	133	40.3248	5.49724	3.4176	2.926	148.3
5	460	45.2800	7.86032	33.151	0.302	17.1
7	330	49.9280	7.92367	26.223	0.381	12.4

[a] The resistivities (ρ) of **2**, **5**, and **7** were obtained depending on the formula of $S/(LG)$ ($S = \pi r^2$, L = length of the single crystals); dielectric constants (ϵ_r) of **2**, **5**, and **7** were obtained depending on the formula of $BL/(2\pi fs)$.

and **L10** and polymeric compounds **1**−**7** were investigated in CH_3CN and the solid state. In the solid-state case, single crystalline samples were used for the measurements. The ground microcrystalline samples were housed in the solid sample quartz carrier. The excitation and emission slit widths are 5 nm. The fluorescence spectra of **L9**, **L10**, and **1**−**7** are summarized in Table 11. As indicated in Figure 29, in CH_3CN, **L9** and **L10** present one maximum at 361 nm for **L9** and 350 nm for **L10**. In the solid state, **L9** and **L10** exhibit one emission maximum at 387 and 386 nm, respectively. In the solid state, as shown in Table 12, the emission colors of the free ligands were significantly affected by their incorporation into the Ag-containing polymeric compounds **1**−**7**, as evidenced by the large shift in the emission. Only slight enhancement of the fluorescence intensity is realized. In CH_3CN, almost no difference has been found between the ligands' and complexes' emission colors. This implies that the polymeric complexes disaggregate into oligomers or starting materials in acetonitrile.

Conclusions

This study demonstrates that the bent oxadiazole bridging benzoacetylene organic ligands 2,5-bis(4-ethynylphenyl)-1,3,4-oxadiazole (**L9**) and 2,5-bis(3-ethynylphenyl)-1,3,4-oxadiazole (**L10**) are capable of coordinating metal centers with both $N_{oxadiazole}$ and terminal −C≡CH π-donors and generate novel organometallic coordination polymers. Seven new polymeric compounds **1**−**7** were synthesized from solution reactions of **L9** and **L10** with various Ag(I) salts. The relative orientation of the π-donors on the phenyl groups and the five-membered oxadiazole spacing in **L9** and **L10** resulted in the unusual building blocks, leading to the construction of polymeric motifs which have not been obtained using normal linear rigid bidentate organic ligands and known bent spacers **L1**−**L8**. The results reported herein demonstrate that the use of organic spacers containing both the −C≡CH moiety and coordinating heterocyclic group as precursors to bind transition metal ions is in fact a new approach for the formation of novel organometallic molecular and supramolecular networks with interesting physical

(23) (a) Kobayashi, A.; Tanaka, H.; Kobayashi, H. *J. Mater. Chem.* **2001**, *11*, 2078. (b) S.-L. Zheng, J.-P. Zhang, W.-T. Wang, X.-M. Chen, *J. Am. Chem. Soc.* **2003**, *125*, 6882.
(24) Bousseau, M.; Valade, L.; Legros, J.-P.; Cassoux, P.; Garbauskas, M.; Interrante, V. *J. Am. Chem. Soc.* **1986**, *108*, 1908.
(25) (a) Ciurtin, D. M.; Pschirer, N. G.; Smith, M. D.; Bunz, U. H. F.; zur Loye, H.-C. *Chem. Mater.* **2001**, *13*, 2743. (b) Cariati, E.; Bu, X.; Ford, P. C. *Chem. Mater.* **2000**, *12*, 3385. (c) Würthner, F.; Sautter, A. *Chem. Commun.* **2000**, 445.
(26) (a) Harvey, P. D.; Gray, H. B. *J. Am. Chem. Soc.* **1988**, *110*, 2145. (b) Catalano, V. J.; Kar, H. M.; Bennett, B. L. *Inorg. Chem.* **2000**, *39*, 121. (c) Tong, M.-L.; Chen, X.-M.; Ye, B.-H.; Ji, L.-N. *Angew. Chem., Int. Ed.* **1999**, *38*, 2237. (d) Burini, A.; Bravi, R.; Jr, J. P. F.; Galassi, R.; Grant, T. A.; Omary, M. A.; Pietroni, B. R.; Staples, R. J. *Inorg. Chem.* **2000**, *39*, 3158. (e) Seward, C.; Jia, W.-L.; Wang, R.-Y.; Enright, G. D.; Wang, S.-N. *Angew. Chem., Int. Ed.* **2004**, *43*, 2933. (f) Yam, V. W.-W.; Lo, K. K.-W. *Chem. Soc. Rev.* **1999**, *28*, 323. (g) Wu, C.-D.; Ngo, H. L.; Lin, W. *Chem. Commun.* **2004**, 1588.
(27) (a) Hu, N.-X.; Esteghamatian, M.; Xie, S.; Popovic, Z.; Hor, A.-M.; Ong, B.; Wang, S.-N. *Adv. Mater.* **1999**, *11*, 1460. (b) de Silva, A. S.; de Silva, M. A. A.; Carvalho, C. E. M.; Antunes, O. A. C.; Herrera, J. O. M.; Brinn, I. M.; Mangrich, A. S. *Inorg. Chim. Acta* **1999**, *292*, 1. (c) Wang, J.; Wang, R.; Yang, J.; Zheng, Z.; Carducci, M. D.; Cayou, T.; Peyghambarian, N.; Jabbour, G. E. *J. Am. Chem. Soc.* **2001**, *123*, 6179.

properties. We are currently expanding this result by preparing new longer symmetric and unsymmetric oxadiazole-containing ligands based on **L9** and **L10** by Pd-catalyzed reactions containing different terminal coordination groups and having different orientations of the terminal coordination sites. New coordination polymers with novel polymeric patterns and interesting chemical and physical properties based on these ligands will be reported soon.

Acknowledgment. We are grateful for financial support from the National Natural Science Foundation of China (Grant No. 20371030) and Shangdong Natural Science Foundation (Grant No. Z2004B01).

Supporting Information Available: Crystallographic data in cif format. This material is available free of charge via the Internet at http://pubs.acs.org.

IC0508223